Quantum noise properties of parametric amplifiers driven by two pump waves

C. J. McKinstrie,[1] S. Radic[2] and M. G. Raymer[3]

[1]*Bell Laboratories, Lucent Technologies, Holmdel, NJ 07733*
[2]*Department of Electrical and Computer Engineering, University of California at San Diego, La Jolla, CA 92093*
[3]*Oregon Center for Optics and Department of Physics, University of Oregon, Eugene, OR 97403*
mckinstrie@lucent.com

Abstract: In a parametric amplifier (PA) driven by two pump waves the signal sideband is coupled to three idler sidebands, all of which are frequency-converted (FC) images of the signal, and two of which are phase-conjugated (PC) images of the signal. If such a device is to be useful, the signal must be amplified, and the PC and FC idlers must be produced, with minimal noise. In this paper the quantum noise properties of two-sideband (TS) parametric devices are reviewed and the properties of many-sideband devices are determined. These results are applied to the study of two-pump PAs, which are based on the aforementioned four-sideband (FS) interaction. As a general guideline, the more sidebands that interact, the higher are the noise levels. However, if the pump frequencies are tuned to maximize the frequency bandwidth of the FS interaction, the signal and idler noise-figures are only slightly higher than the noise figures associated with the limiting TS interactions.

OCIS codes: 060.2320 fiber amplifiers and oscillators, 190.2620 frequency conversion, 190.5040 phase conjugation, 270.2500 fluctuations, relaxations and noise.

References and links

1. K. O. Hill, D. C. Johnson, B. S. Kawasaki and R. I. MacDonald, "CW three-wave mixing in single-mode optical fibers," J. Appl. Phys. **49**, 5098–5106 (1978).
2. R. H. Stolen and J. E. Bjorkholm, "Parametric amplification and frequency conversion in optical fibers," IEEE J. Quantum Electron. **18**, 1062–1072 (1982).
3. C. J. McKinstrie, S. Radic and A. R. Chraplyvy, "Parametric amplifiers driven by two pump waves," IEEE J. Sel. Top. Quantum Electron. **8**, 538–547 and 956 (2002), and references therein.
4. C. J. McKinstrie, S. Radic and C. Xie, "Parametric instabilities driven by orthogonal pump waves in birefringent fibers," Opt. Express **11**, 2619–2633 (2003) and references therein.
5. C. J. McKinstrie, H. Kogelnik, R. M. Jopson, S. Radic and A. V. Kanaev, "Four-wave mixing in fibers with random birefringence," Opt. Express **12**, 2033–2055 (2004) and refrences therein.
6. S. Radic, C. J. McKinstrie, R. M. Jopson, Q. Lin and G. P. Agrawal, "Record performance of a parametric amplifier constructed with highly-nonlinear fiber," Electron. Lett. **39**, 838–839 (2003).
7. T. Tanemura, C. S. Goh, K. Kikuchi and S. Y. Set, "Highly efficient arbitrary wavelength conversion within entire C-band based on nondegenerate fiber four-wave mixing," IEEE Photon. Tech. Lett. **16**, 551–553 (2004).
8. J. M. Manley and H. E. Rowe, "Some general properties of nonlinear elements—Part I. General energy relations,"Proc. IRE **44**, 904–913 (1956).
9. M. T. Weiss, "Quantum derivation of energy relations analogous to those for nonlinear reactances," Proc. IRE **45**, 1012–1013 (1957).
10. W. H. Louisell, A. Yariv and A. E. Siegman, "Quantum fluctuations and noise in parametric processes I," Phys. Rev. **124**, 1646–1654 (1961).

#4717 - $15.00 US Received 1 July 2004; revised 30 September 2004; accepted 1 October 2004

11. J. P. Gordon, W. H. Louisell and L. R. Walker, "Quantum fluctuations and noise in parametric processes II," Phys. Rev. **129**, 481–485 (1963).
12. W. H. Louisell, *Radiation and Noise in Quantum Electronics* (McGraw-Hill, New York, 1964).
13. B. R. Mollow and R. J. Glauber, "Quantum theory of parametric amplification I," Phys. Rev. **160**, 1076–1096 (1967).
14. B. R. Mollow and R. J. Glauber, "Quantum theory of parametric amplification II," Phys. Rev. **160**, 1097–1108 (1967).
15. J. Mostowski and M. G. Raymer, "Quantum statistics in nonlinear optics," in *Contemporary Nonlinear Optics*, edited by G. P. Agrawal and R. W. Boyd (Academic Press, San Diego, 1992), and references therein.
16. R. Loudon, *The Quantum Theory of Light, 3rd Ed.* (Oxford University Press, Oxford, 2000).
17. L. D. Landau, E. M. Lifshitz and L. P. Pitaevskii, *Electrodynamics of Continuous Media, 2nd Ed.* (Butterworth-Heinemann, Oxford, 1984).
18. T. H. Stix, *Waves in Plasmas* (American Institute of Physics, New York, 1992).
19. R. J. Glauber, "Coherent and incoherent states of the radiation field," Phys. Rev. **131**, 2766–2788 (1963).
20. F. T. Arecchi, "Measurement of the statistical distribution of Gaussian and laser sources," Phys. Rev. Lett. **15**, 912–916 (1965).
21. C. Freed and H. A. Haus, "Photoelectron statistics produced by a laser operating below and above the threshold of oscillation," IEEE J. Quantum Electron. **2**, 190–195 (1966).
22. W. Schottky, "On spontaneous current fluctuations in different electrical conductors," Ann. Phys. (Leipzig) **57**, 541–567 (1918).
23. S. Radic and C. J. McKinstrie, "Two-pump fiber parametric amplifiers," Opt. Fiber Technol. **9**, 7–23 (2003).
24. S. Radic, C. J. McKinstrie, R. M. Jopson, A. H. Gnauck, J. C. Centanni and A. R. Chraplyvy, "Multi-band bit-level switching in two-pump fiber parametric devices," IEEE Photon. Technol. Lett. **16**, 852–854 (2004).
25. S. Radic, C. J. McKinstrie, A. R. Chraplyvy, G. Raybon, J. C. Centanni, C. G. Jorgensen, K. Brar and C. Headley, "Continuous-wave parametric-gain synthesis using nondegenerate-pump four-wave mixing," IEEE Photon. Technol. Lett. **14**, 1406–1408 (2002).
26. P. C. Becker, N. A. Olssen and J. R. Simpson, *Erbium-Doped Fiber Amplifiers* (Academic Press, San Diego, 1999).
27. K. Rottwitt and A. J. Stentz, "Raman amplification in lightwave communication systems," in *Optical Fiber Telecommunications IVA*, edited by I. Kaminow and T. Li (Academic Press, San Diego, 2002), pp. 213–257.
28. A. H. Nayfeh, *Introduction to Perturbation Techniques* (Wiley, New York, 1981).

1. Introduction

Long-haul optical communication systems need optical amplifiers to compensate for fiber loss. Current systems use erbium-doped or Raman fiber amplifiers. One could also use parametric fiber amplifiers (PAs), which use four-wave mixing (FWM) enabled by the Kerr nonlinearity to amplify the signals [1, 2]. PAs offer the simultaneous possibilities of broad-bandwidth amplification, wavelength conversion (WC) and impairment reduction by phase conjugation (PC). Current systems use wavelength-division-multiplexing (WDM) to increase the information capacity of each fiber. For typical systems amplifiers must produce uniform gain over (wavelength) bandwidths of 13–51 nm (to amplify 32–128 10-Gb/s channels with wavelength separations of 0.4 nm).

Parametric amplification (which is also denoted by PA) driven by two pump waves (1 and 2) involves four product waves (signal and idler sidebands) that are coupled by three distinct FWM processes, as illustrated in Fig. 1. Suppose that the signal frequency $\omega_{1-} = \omega_1 - \omega$, where ω is the frequency difference (modulation frequency), and let γ denote a photon. Then the modulation interaction (MI) in which $2\gamma_1 \rightarrow \gamma_{1-} + \gamma_{1+}$ produces an idler with frequency $\omega_{1+} = \omega_1 + \omega$, the Bragg-scattering (BS) process in which $\gamma_{1-} + \gamma_2 \rightarrow \gamma_1 + \gamma_{2-}$ produces an idler with frequency $\omega_{2-} = \omega_2 - \omega$ and the PC process in which $\gamma_1 + \gamma_2 \rightarrow \gamma_{1-} + \gamma_{2+}$ produces an idler with frequency $\omega_{2+} = \omega_2 + \omega$. The classical theory of PA driven by two pump waves was reviewed by McKinstrie [3, 4, 5].

PA is driven most strongly when the pumps have parallel polarization vectors. However, the signal gain depends sensitively on the input signal polarization: It is maximal when the signal is polarized parallel to the pumps and is minimal when the signal is polarized perpendicular to the pumps. Because transmission fibers are not polarization maintaining, practical amplifiers

#4717 - $15.00 US Received 1 July 2004; revised 30 September 2004; accepted 1 October 2004

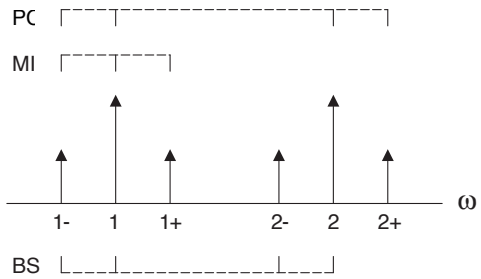

Fig. 1. Illustration of the constituent FWM processes.

must operate on signals with arbitrary polarizations.

PA can also be driven by pumps with perpendicular polarization vectors. In birefringent polarization-maintaining fibers (which we refer to as fibers with constant birefringence) the signal gain depends on the signal polarization. However, in birefringent non-polarization-maintaining fibers (which we refer to as fibers with random birefringence) the random reorientation of the birefringence axes averages out whatever signal-polarization dependence is associated with birefringence: The signal gain (produced by long fibers) does not depend on the input signal polarization. In a recent experiment with a Km-long highly-nonlinear fiber, a gain of 27 dB, with a polarization dependence of 4 dB, was produced over a bandwidth of 34 nm [6].

In most PA experiments the pump wavelengths are tuned to maximize the PC bandwidth. However, by tuning the pump wavelengths in a different way, it is possible to produce WC without amplification (BS) over a bandwidth of 30 nm [7]. This function is also useful for processing applications.

Although much remains to be done to optimize the design and performance of two-pump PAs, the aforementioned results show that they have the potential to meet the basic performance requirements of current communication systems. However, if they are to realize their potential, they must provide amplification with a noise penalty that is comparable to, or lower than, the noise penalty of current (erbium and Raman) amplifiers. In this paper the quantum-noise properties of two-pump PAs are studied in detail.

This paper is organized as follows: In Section 2 the classical equations that model the propagation of light waves in fibers are stated and the associated four-sideband (FS) equations that model two-pump PAs are discussed. For amplifiers operating in the linear regime, the output amplitudes are related to the input amplitudes by a (distance-dependent) transfer matrix. In Sections 3 and 4, respectively, transfer matrices are derived for the two-sideband (TS) interactions (MI, BS and PC), and some special cases of the FS interaction. (These matrices are required in the analysis of the quantum noise properties of PAs.) The transition from the classical model of PAs to the quantum model is described in Section 5. Readers who are familiar with the classical and quantum models of parametric interactions in fibers can proceed directly to Section 6, in which the noise properties of the two-mode processes (MI and PC, and BS) are reviewed. [In the quantum-optics literature these processes are referred to as parametric amplification (PA) and frequency conversion (FC), respectively. Throughout this paper the meaning of the term PA is clear from the context.] In Section 7 the noise properties of many-mode processes are studied. The three-mode process is analyzed explicitly and the results are used to deduce the noise properties of processes that involve an arbitrary number of modes. Because noise is produced by the amplification or combination of the vacuum fluctuations associated with each mode, the noise levels increase in proportion to the number of modes that interact strongly. In Section 8 the

#4717 - $15.00 US Received 1 July 2004; revised 30 September 2004; accepted 1 October 2004

consequences of these results are illustrated for the four-mode processes discussed in Section 4. Finally, in Section 9 the main results of this paper are summarized.

2. Classical equations

In classical mechanics the propagation of two light waves in a fiber is governed by the incoherently-coupled nonlinear Schrödinger (NS) equations

$$-i\partial_z A_1 = \beta_1(i\partial_t)A_1 + \gamma(|A_1|^2 + \varepsilon|A_2|^2)A_1, \quad (1)$$

$$-i\partial_z A_2 = \beta_2(i\partial_t)A_2 + \gamma(\varepsilon|A_1|^2 + |A_2|^2)A_2, \quad (2)$$

where each A_j is the (slowly-varying) amplitude of an electric-field component with carrier frequency ω_j and wavenumber $k_j = k(\omega_j)$, each $\beta_j(\omega) = \sum_{n=1}^{\infty} k_j^{(n)} \omega^n / n!$ represents the higher-order terms in the Taylor expansion of a dispersion function about ω_j, γ is the self-nonlinearity coefficient and ε is the ratio of the cross- and self-nonlinearity coefficients. In polarization-maintaining fibers the birefringence axes (x and y) are fixed in the laboratory frame and $\beta_x \neq \beta_y$. In non-polarization-maintaining fibers the birefringence axes vary randomly with distance along the fiber in the laboratory frame. This random reorientation averages out the effects of birefringence and causes the Stokes vector of a reference wave with frequency ω_0 to rotate randomly. Equations (1) and (2) model wave propagation in both types of fiber, in the laboratory frame, or a frame rotating with the polarization axes of the reference wave. For co-polarized waves $\beta_1 = \beta_2$ and $\varepsilon = 2$ [3]. For cross-polarized waves in fibers with constant birefringence $\beta_1 = \beta_x$, $\beta_2 = \beta_y$ and $\varepsilon = 2/3$ [4], whereas for cross-polarized waves in fibers with random birefringence $\beta_1 = \beta_2$, the self-nonlinearity coefficient is reduced by the factor 9/8 and $\varepsilon = 1$ [5].

The NS equations have an equilibrium solution in which

$$A_1(z) = P_1^{1/2} \exp[i\phi_1(z)], \quad (3)$$

$$A_2(z) = P_2^{1/2} \exp[i\phi_2(z)], \quad (4)$$

where P_1 and P_2 are the pump powers, and the equilibrium phases $\phi_1(z) = \gamma(P_1 + \varepsilon P_2)z$ and $\phi_2(z) = \gamma(\varepsilon P_1 + P_2)z$. Equations (3) and (4) describe two pumps with nonlinear wavenumber shifts imposed by self-phase modulation (SPM) and cross-phase modulation (CPM).

Suppose that the preceding equilibrium is perturbed by a weak signal sideband with frequency $-\omega$ (measured relative to ω_1). As the signal propagates its interaction with pump 1 produces an idler sideband with frequency $+\omega$ (measured relative to ω_1) and its interaction with pump 2 produces idler sidebands with frequencies $\pm\omega$ (measured relative to ω_2). One can manifest this FS interaction by writing

$$A_1(z,t) = [P_1^{1/2} + B_{1+}(z)\exp(-i\omega t) + B_{1-}(z)\exp(i\omega t)]\exp[i\phi_1(z)], \quad (5)$$

$$A_2(z,t) = [P_2^{1/2} + B_{2+}(z)\exp(-i\omega t) + B_{2-}(z)\exp(i\omega t)]\exp[i\phi_2(z)], \quad (6)$$

where $B_{1\pm}$ and $B_{2\pm}$ are the sideband amplitudes. By substituting ansätze (5) and (6) in the NS equations, linearizing the equations that result and collecting terms of like frequency, one obtains the FS equations [3, 4, 5]

$$d_z B_{1-}^* = -i(\beta_{1-} + \gamma P_1)B_{1-}^* - i\gamma P_1 B_{1+} - i\gamma\varepsilon(P_1P_2)^{1/2}B_{2-}^* - i\gamma\varepsilon(P_1P_2)^{1/2}B_{2+}, \quad (7)$$

$$d_z B_{1+} = i\gamma P_1 B_{1-}^* + i(\beta_{1+} + \gamma P_1)B_{1+} + i\gamma\varepsilon(P_1P_2)^{1/2}B_{2-}^* + i\gamma\varepsilon(P_1P_2)^{1/2}B_{2+}, \quad (8)$$

#4717 - $15.00 US Received 1 July 2004; revised 30 September 2004; accepted 1 October 2004

$$
\begin{aligned}
d_z B_{2-}^* &= -i\gamma\varepsilon(P_1P_2)^{1/2}B_{1-}^* - i\gamma\varepsilon(P_1P_2)^{1/2}B_{1+} \\
&\quad - i(\beta_{2-}+\gamma P_2)B_{2-}^* - i\gamma P_2 B_{2+}, \qquad (9)\\
d_z B_{2+} &= i\gamma\varepsilon(P_1P_2)^{1/2}B_{1-}^* + i\gamma\varepsilon(P_1P_2)^{1/2}B_{1+} \\
&\quad + i\gamma P_2 B_{2-}^* + i(\beta_{2+}+\gamma P_2)B_{2+}, \qquad (10)
\end{aligned}
$$

where each wavenumber difference $\beta_{j\pm} = \beta_j(\pm\omega)$.

It follows from Eqs. (7)–(10) that

$$d_z(P_{1-} - P_{1+} + P_{2-} - P_{2+}) = 0. \qquad (11)$$

Equation (11) is the Manley–Rowe–Weiss (MRW) equation [8, 9], which describes the conservation of wave action (photon flux). The appearance of the same nonlinear coefficient in both NS equations was a manifestation of our assumption that the wave frequencies are comparable. In this approximation the proportionality constants that convert powers to action fluxes are also comparable. The MRW equation for action fluxes is exact [5].

3. Classical two-sideband interactions

Because of the complexity of the FS interaction, it is instructive to consider the constituent TS interactions separately. Readers who are familiar with TS and FS interactions in fibers can proceed directly to Section 5.

First, consider the MI in which $2\gamma_1 \to \gamma_{1-} + \gamma_{1+}$. This MI is governed by Eqs. (7) and (8), with the B_{2-}^* and B_{2+} terms omitted. By making the substitutions

$$
\begin{aligned}
B_{1-}^*(z) &= C_{1-}^*(z)\exp[i(\beta_{1+}-\beta_{1-})z/2], \qquad (12)\\
B_{1+}(z) &= C_{1+}(z)\exp[i(\beta_{1+}-\beta_{1-})z/2] \qquad (13)
\end{aligned}
$$

in the MI equations, one can rewrite them in the form

$$
\begin{aligned}
d_z C_{1-}^* &= -i\delta C_{1-}^* - i\kappa C_{1+}, \qquad (14)\\
d_z C_{1+} &= i\kappa C_{1-}^* + i\delta C_{1+}, \qquad (15)
\end{aligned}
$$

where $\delta = (\beta_{1+}+\beta_{1-})/2 + \gamma P_1$ and $\kappa = \gamma P_1$ are the MI mismatch and coupling parameters, respectively. Let C denote the column vector $(C_{1-}^*, C_{1+})^T$. Then the solution of Eqs. (14) and (15) can be written in the matrix form

$$C(z) = M(z)C(0), \qquad (16)$$

where the transfer matrix

$$M(z) = \begin{bmatrix} \cos(kz) - i\delta\sin(kz)/k & -i\kappa\sin(kz)/k \\ i\kappa\sin(kz)/k & \cos(kz) + i\delta\sin(kz)/k \end{bmatrix} \qquad (17)$$

and the MI wavenumber $k = (\delta^2 - \kappa^2)^{1/2}$. The solution described by Eqs. (16) and (17) satisfies the MRW equation

$$d_z(P_{1-} - P_{1+}) = 0 \qquad (18)$$

explicitly. The analysis of the other MI, in which $2\gamma_2 \to \gamma_{2-} + \gamma_{2+}$, is similar.

Second, consider the BS process in which $\gamma_{1-} + \gamma_2 \to \gamma_1 + \gamma_{2-}$. This BS process is governed by Eqs. (7) and (9), with the B_{1+} and B_{2+} terms omitted. By making the substitutions

$$
\begin{aligned}
B_{1-}^*(z) &= C_{1-}^*(z)\exp\{-i[\beta_{2-}+\beta_{1-}+\gamma(P_2+P_1)]z/2\}, \qquad (19)\\
B_{2-}^*(z) &= C_{2-}^*(z)\exp\{-i[\beta_{2-}+\beta_{1-}+\gamma(P_2+P_1)]z/2\} \qquad (20)
\end{aligned}
$$

#4717 - $15.00 US Received 1 July 2004; revised 30 September 2004; accepted 1 October 2004

in the BS equations, one can rewrite them in the form

$$d_z C_{1-} = -i\delta C_{1-} + i\kappa C_{2-}, \quad (21)$$
$$d_z C_{2-} = i\kappa C_{1-} + i\delta C_{2-}, \quad (22)$$

where $\delta = [\beta_{2-} - \beta_{1-} + \gamma(P_2 - P_1)]/2$ and $\kappa = \gamma\varepsilon(P_1 P_2)^{1/2}$ are the BS mismatch and coupling parameters, respectively. The solution of Eqs. (21) and (22) can be written in the form of Eq. (16), provided that the transfer matrix

$$M(z) = \begin{bmatrix} \cos(kz) - i\delta\sin(kz)/k & i\kappa\sin(kz)/k \\ i\kappa\sin(kz)/k & \cos(kz) + i\delta\sin(kz)/k \end{bmatrix} \quad (23)$$

and the BS wavenumber $k = (\delta^2 + \kappa^2)^{1/2}$. The solution described by Eqs. (16) and (23) satisfies the MRW equation

$$d_z(P_{1-} + P_{2-}) = 0 \quad (24)$$

explicitly. The analysis of the other BS process, in which $\gamma_{1+} + \gamma_2 \to \gamma_1 + \gamma_{2+}$, is similar.

Third, consider the PC process in which $\gamma_1 + \gamma_2 \to \gamma_{1-} + \gamma_{2+}$. This PC process is governed by Eqs. (7) and (10), with the B_{1+} and B_{2-}^* terms omitted. By making the substitutions

$$B_{1-}^*(z) = C_{1-}^*(z)\exp\{i[\beta_{2+} - \beta_{1-} + \gamma(P_2 - P_1)]z/2\}, \quad (25)$$
$$B_{2+}(z) = C_{2+}(z)\exp\{i[\beta_{2+} - \beta_{1-} + \gamma(P_2 - P_1)]z/2\} \quad (26)$$

in the PC equations, one can rewrite them in the form

$$d_z C_{1-}^* = -i\delta C_{1-}^* - i\kappa C_{2+}, \quad (27)$$
$$d_z C_{2+} = i\kappa C_{1-}^* + i\delta C_{2+}, \quad (28)$$

where $\delta = [\beta_{2+} + \beta_{1-} + \gamma(P_2 + P_1)]/2$ and $\kappa = \gamma\varepsilon(P_1 P_2)^{1/2}$ are the PC mismatch and coupling parameters, respectively. The solution of Eqs. (27) and (28) can be written in the form of Eq. (16), provided that the transfer matrix

$$M(z) = \begin{bmatrix} \cos(kz) - i\delta\sin(kz)/k & -i\kappa\sin(kz)/k \\ i\kappa\sin(kz)/k & \cos(kz) + i\delta\sin(kz)/k \end{bmatrix} \quad (29)$$

and the PC wavenumber $k = (\delta^2 - \kappa^2)^{1/2}$. The solution described by Eqs. (16) and (29) satisfies the MRW equation

$$d_z(P_{1-} - P_{2+}) = 0 \quad (30)$$

explicitly. For reference, although the PC formulas for the mismatch and coupling parameters [stated after Eq. (28)] differ from the MI formulas [stated after Eq. (15)], the PC transfer matrix (29) has the same form as the MI transfer matrix (17). The analysis of the other PC process, in which $\gamma_1 + \gamma_2 \to \gamma_{1+} + \gamma_{2-}$, is similar.

4. Classical four-sideband interaction

The FS interaction is difficult to analyze, because the equation for the characteristic wavenumbers (eigenvalues) is a fourth-order polynomial that does not have simple solutions. We analyze three special cases of the FS interaction that illustrate its general properties.

Let $B = (B_{1-}^*, B_{1+}, B_{2-}^*, B_{2+})^T$. Then the FS equations (7)–(10) can be written in the matrix form

$$d_z B = LB, \quad (31)$$

#4717 - $15.00 US Received 1 July 2004; revised 30 September 2004; accepted 1 October 2004

where L is a constant matrix. The first tractable case arises when the (dispersive) wavenumber-difference terms ($\beta_{1\pm}$ and $\beta_{2\pm}$) are much larger than the (nonlinear) coupling terms (which are of order γP, where P is a typical pump power). In this case one can solve Eq. (31) perturbatively. Let $L^{(0)} = \mathrm{diag}(-i\beta_{1-}, i\beta_{1+}, -i\beta_{2-}, i\beta_{2+})$, let $\lambda_j^{(0)}$ be an eigenvalue of $L^{(0)}$ and let $L^{(1)} = \left[l_{jk}^{(1)}\right]$ be the matrix of nonlinear coefficients (all of which are proportional to γ). In Appendix A it is shown that

$$B_j(z) \approx B_j(0)\exp\left[\lambda_j^{(0)}z + l_{jj}^{(1)}z\right] + \sum_{k\neq j} B_k(0) l_{jk}^{(1)} \frac{\exp\left[\lambda_k^{(0)}z\right] - \exp\left[\lambda_j^{(0)}z\right]}{\lambda_k^{(0)} - \lambda_j^{(0)}}. \tag{32}$$

Solution (32) can be written in the matrix form

$$B(z) = M(z)B(0), \tag{33}$$

where the transfer matrix $M(z) = [\mu_{jk}(z)]$. It follows from Eqs. (32) and (33) that

$$\mu_{jk}(z) \approx \begin{cases} \exp\left[\lambda_j^{(0)}z + l_{jj}^{(1)}z\right] & \text{if } k = j, \\ l_{jk}^{(1)} \dfrac{\exp\left[\lambda_k^{(0)}z\right] - \exp\left[\lambda_j^{(0)}z\right]}{\lambda_k^{(0)} - \lambda_j^{(0)}} & \text{if } k \neq j. \end{cases} \tag{34}$$

The diagonal elements of the transfer matrix (34) are of order unity. The non-diagonal elements are small, as required by perturbation theory, unless $|\lambda_k^{(0)} - \lambda_j^{(0)}| \sim \gamma P$. It is instructive to consider these resonance conditions further. For MI $\lambda_2^{(0)} - \lambda_1^{(0)} = i(\beta_{1+} + \beta_{1-}) \approx i\beta_1^{(2)}\omega^2$, for BS $\lambda_3^{(0)} - \lambda_1^{(0)} = i(\beta_{1-} - \beta_{2-}) \approx i\left[\beta_2^{(1)} - \beta_1^{(1)}\right]\omega + i\left[\beta_1^{(2)} - \beta_2^{(2)}\right]\omega^2/2$ and for PC $\lambda_4^{(0)} - \lambda_1^{(0)} = i(\beta_{2+} + \beta_{1-}) \approx i\left[\beta_2^{(1)} - \beta_1^{(1)}\right]\omega + i\left[\beta_2^{(2)} + \beta_1^{(2)}\right]\omega^2/2$. Each eigenvalue difference $\lambda_k^{(0)} - \lambda_j^{(0)}$ associated with the approximate solution (32) equals one of the mismatch parameters associated with the TS limits of the FS interaction, which were analyzed in Section 3. It is clear from the preceding formulas that MI is wavenumber matched over a broad bandwidth when $\beta_j^{(2)}\omega^2 \sim \gamma P$, where $j = 1$ or 2. BS is wavenumber matched when $\beta_2^{(1)} \approx \beta_1^{(1)}$ and $\left[\beta_1^{(2)} - \beta_2^{(2)}\right]\omega^2/2 \sim \gamma P$, and PC is wavenumber matched when $\beta_2^{(1)} \approx \beta_1^{(1)}$ and $\left[\beta_2^{(2)} + \beta_1^{(2)}\right]\omega^2/2 \sim \gamma P$: Group-speed matching is a necessary, but insufficient, condition for a strong BS or PC interaction. Although solution (32) provides a guide to the conditions required for PA, it is not directly applicable to PA because it is limited to gains of order 1. However, it is directly relevant to some quantum-mechanical aspects of FS interactions, for which perturbation analyses are sufficient.

The second tractable case arises when the modulation frequency ω is low. In this case $\beta_{1\pm} \approx 0$ and $\beta_{2\pm} \approx 0$. For simplicity, suppose that $P_1 = P_2 = P$. In Appendix A it is shown that the solution of Eq. (31) can be written in the form of Eq. (33), where the transfer matrix

$$M(z) \approx \begin{bmatrix} 1 - i\gamma Pz & -i\gamma Pz & -i\gamma\varepsilon Pz & -i\gamma\varepsilon Pz \\ i\gamma Pz & 1 + i\gamma Pz & i\gamma\varepsilon Pz & i\gamma\varepsilon Pz \\ -i\gamma\varepsilon Pz & -i\gamma\varepsilon Pz & 1 - i\gamma Pz & -i\gamma Pz \\ i\gamma\varepsilon Pz & i\gamma\varepsilon Pz & i\gamma Pz & 1 + i\gamma Pz \end{bmatrix}. \tag{35}$$

It follows from Eqs. (33) and (35) that the sideband powers increase *quadratically* with distance. Although the neglect of dispersion limits the applicability of the solution to an angular-frequency range of a few Trad/s (centered on the pump frequencies), the quadratic growth it

#4717 - $15.00 US Received 1 July 2004; revised 30 September 2004; accepted 1 October 2004

predicts is both ubiquitous (occurs for arbitrary pump frequencies) and significant (10–20 dB in typical experiments [6]).

The third tractable case arises when $\beta_2^{(1)} \approx \beta_1^{(1)}$ and $\beta_2^{(2)} \approx \beta_1^{(2)}$. As discussed above, the first condition (group-speed matching) allows PC to be wavenumber matched and the second condition ensures that the PC matching-condition is similar to the MI matching-condition: All four sidebands are driven near-resonantly, so a strong FS interaction occurs. For example, these conditions are satisfied by two cross-polarized pumps with similar frequencies in fibers with constant birefringence [4] and random birefringence. Let β_e denote the (common) second-order dispersion term $\beta^{(2)}\omega^2/2$ and, for simplicity, suppose that $P_1 = P_2 = P$. Then analysis shows that the FS interaction is unstable when $-2\gamma(1+\varepsilon)P < \beta_e < 0$ and the spatial growth rate attains its maximal value $\kappa_+ = \gamma(1+\varepsilon)P$ when $\beta_e = -\gamma(1+\varepsilon)P$ [4]. In Appendix A the solution of Eq. (31) is derived for this case. In the long-distance limit ($\kappa_+ z \gg 1$) the transfer matrix

$$M(z) \approx \begin{bmatrix} \mu(z) & -i\mu(z) & \mu(z) & -i\mu(z) \\ i\mu(z) & \mu(z) & i\mu(z) & \mu(z) \\ \mu(z) & -i\mu(z) & \mu(z) & -i\mu(z) \\ i\mu(z) & \mu(z) & i\mu(z) & \mu(z) \end{bmatrix}, \tag{36}$$

where the transfer function $\mu(z) = \exp(\kappa_+ z)/4$. It follows from Eqs. (33) and (36) that the sideband powers increase *exponentially* with distance.

Broad-bandwidth PC occurs when $\beta_2^{(2)} \approx -\beta_1^{(2)}$. This condition requires the pump frequencies to be located symmetrically relative to the zero-dispersion frequency. For this case the solution of Eq. (31) is complicated. Nonetheless, it is included in Appendix A for completeness. The symmetry properties of the general solution of Eq. (31) are discussed in Appendix B.

5. Transition from classical to quantum mechanics

The quantum-mechanical aspects of PA were studied first in the context of coupled cavity modes [10, 11, 12, 13, 14]. Such modes have well-defined spatial structures (eigenfunctions) and amplitudes that evolve in time. In classical mechanics one obtains amplitude time-evolution equations by applying the Hamilton equations-of-motion to the classical Hamiltonian. To convert from the classical analysis to the quantum analysis one replaces the mode amplitudes A_j and A_j^* in the classical Hamiltonian by the annihilation and creation operators $\hat{a}_j$ and $\hat{a}_j^\dagger$ in the quantum Hamiltonian. These mode operators are normalized in such a way that $\hat{a}_j^\dagger \hat{a}_j$ measures the number of photons in mode j, and obey the boson commutation relation

$$[\hat{a}_j, \hat{a}_k^\dagger] = \delta_{jk}, \tag{37}$$

where δ_{jk} is the Kronecker delta. One obtains operator time-evolution equations by applying the Heisenberg equation-of-motion to the quantum Hamiltonian. The evolution equations for the quantum operators and the classical amplitudes are the same: Quantum-mechanical effects arise because the annihilation and creation operators do not (all) commute.

In fibers and other open systems, coupled waves grow (or attenuate) as they convect. Such evolution is described in terms of wave packets (collections of modes) rather than (individual) modes. The derivation of quantum-mechanical equations for the parametric interaction of optical pulses in dispersive nonlinear media was described in detail by Mostowski and Raymer [15], and Loudon [16]. In this section the quantization procedure is reviewed briefly. Readers who are familiar with it can proceed directly to Section 6.

Consider the propagation of a linearly-polarized pulse in a linear dielectric medium. Such a pulse can be described as a superposition of plane waves, parameterized by the wavenumber k.

#4717 - $15.00 US Received 1 July 2004; revised 30 September 2004; accepted 1 October 2004

In an (idealized) infinite medium the wavenumber is a continuous variable. The propagation of each Fourier component of the electromagnetic field is characterized by the dispersion function

$$D(\omega,k) = \omega^2 n^2(\omega) - c^2 k^2, \tag{38}$$

where $n(\omega)$ is the index of refraction. The dispersion equation $D(\omega,k) = 0$ defines ω as a function of k or, equivalently, k as a function of ω. It is customary to adopt the latter perspective, even though the former provides a direct link to the Heisenberg equation.

Suppose that the pulse has a narrow frequency spectrum centered about its carrier frequency ω_0. Then it is convenient to write $E = E_+ + E_-$ and $B = B_+ + B_-$, where the positive-frequency fields

$$E_+(t,z) = E_0(t,z)\exp[i\phi_0(t,z)], \tag{39}$$
$$B_+(t,z) = B_0(t,z)\exp[i\phi_0(t,z)] \tag{40}$$

and the negative-frequency fields $E_- = E_+^*$ and $B_- = B_+^*$. In Eqs. (39) and (40) the carrier phase $\phi_0(t,z) = k_0 z - \omega_0 t$ and the carrier wavenumber $k_0 = k(\omega_0)$. In the narrow-bandwidth approximation the field amplitudes E_0 and B_0 vary slowly compared to the carrier phase, and are related by the equation $B_0 = n_0 E_0$, where $n_0 = n(\omega_0)$. By following a standard procedure [17, 18], one can write the energy-conservation equation in the form

$$\partial_t T_0 + \partial_z S_0 = 0, \tag{41}$$

where

$$T_0 = (\partial D/\partial\omega)_0 |E_0|^2/4\pi\omega_0, \tag{42}$$
$$S_0 = -(\partial D/\partial k)_0 |E_0|^2/4\pi\omega_0 \tag{43}$$

are the slowly-varying energy density and energy-density (Poynting) flux, respectively. It follows from Eqs. (41)–(43) that energy convects at the carrier group-speed $v_0 = -(\partial D/\partial k)_0/(\partial D/\partial\omega)_0$.

In quantum mechanics the slowly-varying fields E_0 and B_0 are replaced by the slowly-varying field operators

$$\widehat{E}_0(t,z) = (2\pi\hbar\omega_0/n_0 c)^{1/2}\int \hat{a}(\omega)\exp[i\beta(\omega)z - i\omega t]d\omega/(2\pi)^{1/2}, \tag{44}$$

$$\widehat{B}_0(t,z) = (2\pi\hbar\omega_0 n_0/c)^{1/2}\int \hat{a}(\omega)\exp[i\beta(\omega)z - i\omega t]d\omega/(2\pi)^{1/2}, \tag{45}$$

where ω denotes the relative frequency (difference between the absolute and carrier frequencies) and $\beta(\omega)$ is the Taylor expansion of the relative wavenumber $k - k_0$. [In the narrow-bandwidth approximation $\beta = \omega/v_0$. The higher-order terms are retained for use in other contexts.] Factors of $A_\perp^{1/2}$, where $A_\perp$ is the effective area of the fiber, were absorbed into the field operators, to allow the associated energy densities to be measured per unit length. The annihilation and creation operators obey the commutation relation

$$[\hat{a}(\omega), \hat{a}^\dagger(\omega')] = \delta(\omega - \omega'), \tag{46}$$

which is the continuous version of the discrete relation (37). By combining Eqs. (42) and (44), and using the identity $\delta[\beta(\omega) - \beta(\omega')] = v_0\delta(\omega - \omega')$, one finds that the pulse-energy operator

$$\int \widehat{T}_0(t,z)dz = \hbar\omega_0 \int \hat{a}^\dagger(\omega)\hat{a}(\omega)d\omega. \tag{47}$$

#4717 - $15.00 US Received 1 July 2004; revised 30 September 2004; accepted 1 October 2004

(The zero-point terms were omitted.) It follows from Eq. (47) that $\hat{a}^\dagger(\omega)\hat{a}(\omega)$ has units of photon number per unit frequency.

The form of Eq. (44) makes it natural to define the slowly-varying (frequency-domain) operator

$$\hat{a}(\omega,z) = \hat{a}(\omega)\exp[i\beta(\omega)z] \tag{48}$$

and its Fourier transform, the slowly-varying (time-domain) operator

$$\hat{a}(t,z) = \int \hat{a}(\omega)\exp[i\beta(\omega)z - i\omega t]d\omega/(2\pi)^{1/2}. \tag{49}$$

It follows from the Parseval equation

$$\int \hat{a}^\dagger(t,z)\hat{a}(t,z)dt = \int \hat{a}^\dagger(\omega,z)\hat{a}(\omega,z)d\omega \tag{50}$$

that $\hat{a}^\dagger(t,z)\hat{a}(t,z)$ has units of photon number per unit time (photon flux). By combining Eqs. (46), (48) and (49), one finds that the slowly-varying operators obey the commutation relations

$$[\hat{a}(\omega,z),\hat{a}^\dagger(\omega',z)] = \delta(\omega-\omega'), \tag{51}$$

$$[\hat{a}(t,z),\hat{a}^\dagger(t',z)] = \delta(t-t'). \tag{52}$$

It follows from Eq. (49) that

$$-i\partial_z\hat{a} = \beta(i\partial_t)\hat{a}, \tag{53}$$

which is a linear Schrödinger equation. [In the narrow-bandwidth approximation Eq. (53) is the convection equation.]

Power is defined to be the average rate at which energy arrives at a detector during a time interval that is much longer than $1/\omega_0$. By combining Eqs. (43) and (44) one finds that the energy-flux operator

$$\widehat{S}_0(t,z) = \hbar\omega_0\hat{a}^\dagger(t,z)\hat{a}(t,z) \tag{54}$$

(The formula for this operator does not contain zero-point terms.) It follows from Eq. (54) that the number operator for photons detected during the time interval T is

$$\hat{m}_T(t,z) = \int_{t-T/2}^{t+T/2} \hat{a}^\dagger(t',z)\hat{a}(t',z)dt'. \tag{55}$$

Equation (55) is consistent with Eq. (50), which identified $\hat{a}^\dagger(t,z)\hat{a}(t,z)$ as the photon-flux operator.

Equation (53) describes how the slowly-varying operator $\hat{a}(t,z)$ evolves and Eq. (55) describes how it is related to the measurement of photons. The result of such a measurement depends on the quantum state of the field. It is customary to assume that the field is in a coherent state [19], because a coherent state is a minimal-uncertainty state [10, 19] and is the state produced by an ideal, single-mode laser operating well-above threshold [20, 21]. The continuous-mode coherent state $|\{\alpha\}\rangle$ is related to the vacuum state $|\{0\}\rangle$ by the equation

$$|\{\alpha\}\rangle = \exp(\hat{a}_\alpha^\dagger - \hat{a}_\alpha)|\{0\}\rangle, \tag{56}$$

where $\{\ \}$ denotes a set of state parameters [$\alpha(\omega)$ or 0], the wave-packet creation operator

$$\hat{a}_\alpha^\dagger = \int \alpha(\omega)\hat{a}^\dagger(\omega)d\omega \tag{57}$$

#4717 - $15.00 US Received 1 July 2004; revised 30 September 2004; accepted 1 October 2004

and $\hat{a}_\alpha$ is the associated wave-packet annihilation operator. It follows from Eqs. (56) and (57) that $|\alpha(\omega)|^2$ has units of photon number per unit frequency. Definition (57) can be rewritten in the form

$$\hat{a}_\alpha^\dagger = \int \alpha(\omega,z)\hat{a}^\dagger(\omega,z)d\omega, \tag{58}$$

where $\hat{a}^\dagger(\omega,z)$ is the distance-dependent operator defined by Eq. (48) and

$$\alpha(\omega,z) = \alpha(\omega)\exp[i\beta(w)z] \tag{59}$$

is the distant-dependent coherent-state function. By applying a standard procedure [16] to Eq. (56), one finds that

$$\hat{a}(\omega,z)|\{\alpha\}\rangle = \alpha(\omega,z)|\{\alpha\}\rangle, \tag{60}$$

$$\hat{a}(t,z)|\{\alpha\}\rangle = \alpha(t,z)|\{\alpha\}\rangle, \tag{61}$$

where $\alpha(t,z)$ is the inverse Fourier transform of $\alpha(\omega,z)$. Equations (60) and (61) identify the coherent state $|\{\alpha\}\rangle$ as an eigenstate of the slowly-varying annihilation operator $\hat{a}$.

Let $\overline{m}_T = \langle\{\alpha\}|\hat{m}_T|\{\alpha\}\rangle$ be the expected (mean) value of the measured photon number. Then it follows from Eqs. (55) and (61) that, for a coherent state,

$$\overline{m}_T(t,z) = \int_{t-T/2}^{t+T/2} |\alpha(t',z)|^2 dt'. \tag{62}$$

Equation (62) identifies $|\alpha(t,z)|^2$ as the photon flux of a coherent state. Let $\delta m_T^2 = \langle\hat{m}_T^2\rangle - \langle\hat{m}_T\rangle^2$ be the variance of the measured photon number. Then it follows from Eqs. (52), (55) and (61) that

$$\delta m_T^2(t,z) = \overline{m}_T(t,z). \tag{63}$$

This photon-number uncertainty is responsible for shot noise [22] in an ideal detector.

The preceding paragraphs describe the propagation and detection of an isolated pulse. In a PA two strong, coherent pump pulses interact with four weak product pulses. This interaction is made possible by the Kerr nonlinearity of the fiber. It is customary to model the pumps classically ($P_j = \hbar\omega_j|\alpha_j|^2$) and the products quantum-mechanically. In this model the products are governed by Eqs. (7)–(10), in which the (phase-shifted) amplitudes B_j and B_j^* are replaced by the (interaction-picture) operators $\hat{a}_j$ and $\hat{a}_j^\dagger$, and the spatial derivatives d_z are replaced by the convective derivatives $\partial_z + \partial_t/v_j$. Once these operator equations are solved, the output photon-numbers and photon-number variances of the four product pulses are found from Eq. (55).

In the context of this paper, it is sufficient to consider the interaction of long pulses (quasi-continuous waves). For such pulses the differences in group speed can be neglected. By defining the (common) retarded time $t - z/v$, one can replace the convective derivatives in the operator equations by spatial derivatives: Long pulses are governed by Eqs. (7)–(10). Consequently, the transfer matrices that relate the input and output operators are the same as the transfer matrices that relate the input and output amplitudes, which were described in Sections 3 and 4.

For long pulses the quantization procedure and measurement analysis also simplify considerably. Let L be the system (quantization) length. Then the mode wavenumbers are integral multiples of $2\pi/L$, the mode frequencies are multiples of $\Delta = 2\pi v/L$ and the discrete-mode operators

$$\hat{a}_k = \int_{\omega_k-\Delta/2}^{\omega_k+\Delta/2} \hat{a}(\omega)d\omega/\Delta^{1/2}. \tag{64}$$

It follows from Eq. (64) that $\hat{a}_k^\dagger\hat{a}_k$ has units of photon number. By combining Eqs. (46) and (64), one finds that

$$[a_k, a_l^\dagger] = \delta_{kl}, \tag{65}$$

#4717 - $15.00 US Received 1 July 2004; revised 30 September 2004; accepted 1 October 2004

which is the analog of Eq. (37). It follows from Eqs. (49) and (64) that

$$\hat{a}_j(t,z) = (v/L)^{1/2} \sum_k \hat{a}_k \exp[i\beta(\omega_k)z - i\omega_k t]. \tag{66}$$

Because each wave is quasi-monochromatic, the summation in Eq. (66) only includes modes for which $\omega_k \approx \omega_j$. The factor of $(v/L)^{1/2}$ converts photon numbers to photon fluxes. By combining Eqs. (55) and (66), one finds that for each wave

$$\hat{m}_T(t,z) = (Tv/L) \sum_{k,l} \mathrm{sinc}(\omega_{lk}T/2)\hat{a}_k^\dagger \hat{a}_l \exp(i\beta_{lk}z - i\omega_{lk}t), \tag{67}$$

where $\beta_{lk} = \beta(\omega_l) - \beta(\omega_k)$ and $\omega_{lk} = \omega_l - \omega_k$.

The single-mode coherent state $|\alpha_j\rangle$ is related to the vacuum state $|0\rangle$ by the equation

$$|\alpha_j\rangle = \exp(\alpha_j \hat{a}_j^\dagger - \alpha_j^* \hat{a}_j)|0\rangle. \tag{68}$$

By applying a standard procedure [16] to Eq. (68), one finds that

$$\hat{a}_j|\alpha_j\rangle = \alpha_j|\alpha_j\rangle, \tag{69}$$

which identifies $|\alpha_j\rangle$ as an eigenstate of $\hat{a}_j$. Let $|\alpha_j, 0\rangle$ denote the state in which mode j is a coherent state and the other (neighboring) modes are all vacuum states. Then it follows from Eqs. (67) and (69), and the fact that $\hat{a}_k|\alpha_j, 0\rangle = 0$ if $k \neq j$, that

$$\overline{m}_T = (Tv/L)\overline{m}_j, \tag{70}$$

where $\overline{m}_j = |\alpha_j|^2$ is the (mean) number of photons in mode j. It follows from Eqs. (67) and (69), and the inequality $Tv/L \ll 1$, that

$$\delta m_T^2 = \overline{m}_T. \tag{71}$$

Equation (71) is identical to Eq. (63): The photon-number uncertainty, which plays a fundamental role in the noise-figure analysis, is a general property of any coherent-state wavepacket, and is not an artifact of the (idealized) single-mode model. Despite the simplicity of the single-mode model, it cannot be adopted at the outset because the mode wavenumbers are real by construction and, hence, do not allow the product waves to grow as they propagate (and interact with the pump waves).

There are many similarities between the temporal growth of cavity modes and the convective growth of long pulses: In the former process the mode operators evolve in time and one measures the number of photons in each mode. In the latter process the slowly-varying mode operators evolve in time and distance and one averages each photon flux over the measurement time T. If the pulses convect at a common group speed, one can (phenomenologically) replace the time variable t by the distance variable z/v. In the single-mode model each measured photon number is proportional to the number of photons in that mode [$\overline{m}_T = (Tv/L)m_j$]. In Sections 6–8 we use the language of the cavity-mode interaction to describe the interaction of long pulses. This language simplifies our discussions of two- and four-mode interactions, and ties them to the original discussions of PA and FC. It should be clear from the preceding discussion that the simplification is linguistic: The results are valid for cavity-mode and long-pulse interactions.

6. Quantum two-mode processes

Equations (16), (17) and (29) describe classical versions of a two-mode quantum process in which a creation operator is coupled to an annihilation operator. Such a process, which is called PA in the quantum-optics literature, is governed by the matrix equation

$$B = MA, \tag{72}$$

#4717 - $15.00 US Received 1 July 2004; revised 30 September 2004; accepted 1 October 2004

where the input vector $A = (a_1^\dagger, a_2)^T$, the output vector $B = (b_1^\dagger, b_2)^T$, the transfer matrix

$$M(z) = \begin{bmatrix} \mu^*(z) & \nu^*(z) \\ \nu(z) & \mu(z) \end{bmatrix} \tag{73}$$

and the operator symbols $\hat{}$ were omitted for simplicity of notation. Different symbols were used for the input and output vectors to obviate the need to specify the input and output locations explicitly. The vector B also represents the intermediate states of the system at all positions within the PA. In $\chi^{(3)}$ media, such as fibers, PA can be driven by one or two pumps. In the former case the two-mode model is complete, whereas in the latter it is a simplification of the four-mode model (Sections 7 and 8). In $\chi^{(2)}$ media PA is driven by one pump and the two-mode model is complete [12].

In the interaction picture the operators evolve. However, the commutators are constants of the motion: $[b_j, b_k] = [a_j, a_k] = 0$ and $[b_j, b_k^\dagger] = [a_j, a_k^\dagger] = \delta_{jk}$. By evaluating the commutator $[b_1, b_1^\dagger]$ (or $[b_2, b_2^\dagger]$) one finds that

$$|\mu|^2 - |\nu|^2 = 1. \tag{74}$$

The other commutation relations provide no additional information. Equation (74) is the quantum analog of the MRW equation (18). The transformation described by Eqs. (72)–(74) is called a two-mode squeezing transformation [15].

Let $n_j = b_j^\dagger b_j$ denote the output-number operator of mode j. Then it follows from Eqs. (72) and (73) that

$$n_1 = |\mu|^2 a_1^\dagger a_1 + |\nu|^2 a_2 a_2^\dagger + \mu^* \nu a_1^\dagger a_2^\dagger + \mu \nu^* a_2 a_1, \tag{75}$$

$$n_2 = |\nu|^2 a_1 a_1^\dagger + |\mu|^2 a_2^\dagger a_2 + \mu \nu^* a_1 a_2 + \mu^* \nu a_2^\dagger a_1^\dagger. \tag{76}$$

For reference, one can deduce formula (76) from formula (75) by interchanging the subscripts 1 and 2, and taking the hermitian conjugate of the formula that results.

Suppose that the initial condition of the system is an energy (number) eigenstate with m_1 quanta of mode 1 and m_2 quanta of mode 2, which is denoted by $|m_1, m_2\rangle$. (Such a state is of interest because it has simple properties that facilitate the illustration of quantum effects in PA, and is a building block for coherent states.) Then the expected value (mean) of the output number of mode j is $\langle m_1, m_2 | n_j | m_1, m_2 \rangle$. Because different number eigenstates are orthogonal, it follows from Eqs. (75) and (76) that

$$\langle n_1 \rangle = |\mu|^2 m_1 + |\nu|^2 (m_2 + 1), \tag{77}$$

$$\langle n_2 \rangle = |\nu|^2 (m_1 + 1) + |\mu|^2 m_2. \tag{78}$$

Because the creation and annihilation operators of mode k do not commute, the output of mode $j \neq k$ includes the quantum contribution $1|\nu|^2$. This contribution is what one would predict classically, by adding 1 noise photon to mode k.

Not only do quantum effects contribute to the means of the output numbers, they also contribute to their variances, which are proportional to the variances of electrical currents in a receiver. It follows from Eq. (75) that the second-moment operator

$$\begin{aligned} n_1^2 = {} & (|\mu|^2 a_1^\dagger a_1 + |\nu|^2 a_2 a_2^\dagger)^2 + (\mu^* \nu a_1^\dagger a_2^\dagger + \mu \nu^* a_2 a_1)^2 \\ & + (|\mu|^2 a_1^\dagger a_1 + |\nu|^2 a_2 a_2^\dagger)(\mu^* \nu a_1^\dagger a_2^\dagger + \mu \nu^* a_2 a_1) \\ & + (\mu^* \nu a_1^\dagger a_2^\dagger + \mu \nu^* a_2 a_1)(|\mu|^2 a_1^\dagger a_1 + |\nu|^2 a_2 a_2^\dagger). \end{aligned} \tag{79}$$

The output-number variance $\langle \delta n_1^2 \rangle = \langle n_1^2 \rangle - \langle n_1 \rangle^2$. The first term on the right side of Eq. (79) contributes $\langle n_1 \rangle^2$ to the variance, which cancels the $-\langle n_1 \rangle^2$ term in its definition. Because

#4717 - $15.00 US Received 1 July 2004; revised 30 September 2004; accepted 1 October 2004

different number eigenstates are orthogonal, the third and fourth terms in Eq. (79) contribute nothing. Hence, the variance is determined solely by the second term on the right side of Eq. (79). It follows from these observations that

$$\langle \delta n_1^2 \rangle = |\mu|^2 |\nu|^2 (2m_1 m_2 + m_1 + m_2 + 1). \tag{80}$$

The terms $m_1 + m_2 + 1$ are present in Eq. (80) because the creation and annihilation operators of modes 1 and 2 do not commute. It follows from the symmetry described after Eq. (76) that $\langle \delta n_2^2 \rangle = \langle \delta n_1^2 \rangle$. For the case in which mode 1 is a signal ($m_1 \neq 0$) and mode 2 is an idler ($m_2 = 0$), $\langle \delta n_j^2 \rangle = |\mu|^2 |\nu|^2 (m_1 + 1)$. In many systems $m_1 \gg 1$, even if the signal is classically weak. In such systems the quantum contribution to the (common) output-number variance, which we call the quantum noise, is what one would predict classically, by adding 1/2 of a noise photon to mode 2. The manifestation of this photon-number uncertainty in a receiver is called the signal–spontaneous beat noise.

The preceding results were obtained for an idealized signal with zero input-number variance. However, a realistic signal has a nonzero input-number variance. As noted in Section 5, it is customary to assume that the input signal is a coherent state, because a coherent state is a minimal-uncertainty state and is the state produced by a laser operating above threshold. Such a signal is called a shot-noise-limited signal, because its intrinsic photon-number uncertainty is responsible for shot noise in an ideal receiver. The wavefunction of a (single-mode) coherent state was defined implicitly by Eq. (68). Suppose that the input signal (mode 1) is a coherent state, characterized by the parameter $\alpha_1 = \overline{m}_1^{1/2} \exp(i\phi_1)$, and there is no input idler. Then the input wavefunction has the explicit representation

$$|\psi\rangle = \sum_{m_1=0}^{\infty} [p(m_1)]^{1/2} \exp(im_1\phi) |m_1, 0\rangle, \tag{81}$$

where $p(m) = \overline{m}^m \exp(-\overline{m})/m!$ is a Poisson distribution with mean $\overline{m}$ [10, 19]. It follows from Eqs. (75), (76) and (81) that, in this case, the output-number means

$$\langle n_1 \rangle = |\mu|^2 \overline{m}_1 + |\nu|^2, \tag{82}$$

$$\langle n_2 \rangle = |\nu|^2 (\overline{m}_1 + 1). \tag{83}$$

A Poisson distribution with mean $\overline{m}$ also has variance $\overline{m}$. This uncertainty adds $|\mu|^4 \overline{m}_1$ to the first term in Eq. (79) and $|\nu|^4 \overline{m}_1$ to the first term in the analogous equation for mode 2. Although $\langle m_1, 0 | n_1, 0 \rangle \neq 0$ for a Poisson state, the other terms in Eq. (79) contain unbalanced powers of $a_2^{(\dagger)}$, so the associated inner products remain zero. Hence, in this case, the output-number variances

$$\langle \delta n_1^2 \rangle = |\mu|^4 \overline{m}_1 + |\mu|^2 |\nu|^2 (\overline{m}_1 + 1), \tag{84}$$

$$\langle \delta n_2^2 \rangle = |\nu|^4 \overline{m}_1 + |\mu|^2 |\nu|^2 (\overline{m}_1 + 1). \tag{85}$$

By comparing Eqs. (84) and (85) with the $m_2 = 0$ limits of Eq. (80) and its analog for mode 2, one finds that the input uncertainty adds to the output uncertainties, but does not otherwise change the PA process. The preceding results were obtained first by Louisell [10].

At any position within the PA the signal-to-noise ratio (SNR) of mode j is defined as $\langle n_j \rangle^2 / \langle \delta n_j^2 \rangle$. The signal noise-figure F_1 is defined as the ratio of the input and output SNRs of the signal (mode 1). A useful feature of a PA is its ability to generate an idler that is a phase-conjugated image of the signal. In this context, we define the idler noise-figure F_2 as the ratio of the input SNR of the signal divided by the output SNR of the idler (mode 2). Let

#4717 - $15.00 US Received 1 July 2004; revised 30 September 2004; accepted 1 October 2004

$G = |\mu|^2$ denote the signal gain. Then $|\nu|^2 = G - 1$. It follows from Eqs. (82)–(85) that the PA noise-figures

$$F_1 = \frac{\overline{m}_1[G^2\overline{m}_1 + G(G-1)(\overline{m}_1+1)]}{[G\overline{m}_1 + (G-1)]^2}, \tag{86}$$

$$F_2 = \frac{\overline{m}_1[(G-1)^2\overline{m}_1 + G(G-1)(\overline{m}_1+1)]}{(G-1)^2(\overline{m}_1+1)^2}. \tag{87}$$

In the high-gain limit ($G \gg 1$) $F_j = \overline{m}_1(2\overline{m}_1+1)/(\overline{m}_1+1)^2 \approx 2$ (3 dB). The PA noise-figures are plotted as functions of distance in Fig. 2 for the case in which $\overline{m}_1 \gg 1$ and $\delta = 0$. [See Eqs. (17) and (29).] The signal noise-figure increases monotonically from 1 to 2, whereas the idler

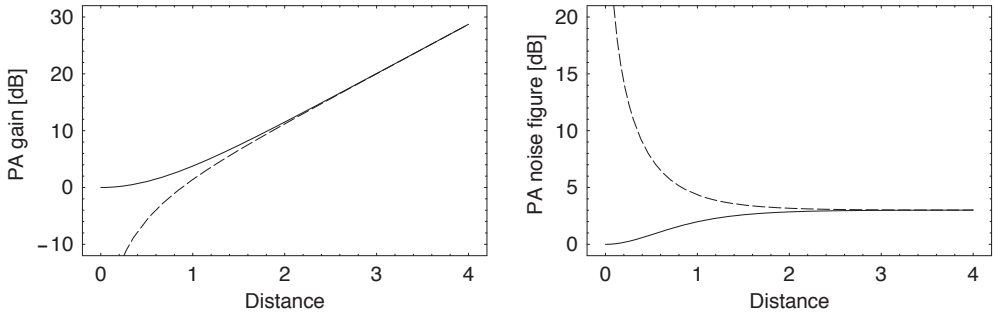

Fig. 2. Gains and noise figures of a two-mode parametric amplifier. The solid curves represent the signal, whereas the dashed curves represent the idler. Distance is normalized to the gain length $[\gamma\varepsilon(P_1P_2)^{1/2}]^{-1}$.

noise-figure decreases monotonically from ∞ to 2. For distances longer than 2 gain lengths the noise figures are comparable. The results for $\delta \neq 0$ are similar.

Equations (16) and (23) describe the classical version of a two-mode quantum process in which two annihilation (or creation) operators are coupled. Such a process, which is called FC in the quantum-optics literature, is also governed by an equation of the form (72), in which the input vector $A = (a_1, a_2)^T$, the output vector $B = (b_1, b_2)^T$ and the transfer matrix

$$M(z) = \begin{bmatrix} \mu(z) & \nu(z) \\ -\nu^*(z) & \mu^*(z) \end{bmatrix}. \tag{88}$$

In $\chi^{(2)}$ media FC is driven by one pump and the two-mode model is complete [12]. In $\chi^{(3)}$ media, such as fibers, (nondegenerate) FC is driven by two pumps and the two-mode model is a simplification of the four-mode model (Sections 7 and 8).

By evaluating the commutator $[b_1, b_1^\dagger]$ (or $[b_2, b_2^\dagger]$) one finds that

$$|\mu|^2 + |\nu|^2 = 1. \tag{89}$$

The other commutation relations provide no additional information. Equation (89) is the quantum analog of the MRW equation (24). The transformation described by Eqs. (72), (88) and (89) is called a beam-splitter transformation [16]. (In the context of FC this transformation is accompanied by a frequency shift.)

It follows from Eqs. (72) and (88) that the output-number operators

$$n_1 = |\mu|^2 a_1^\dagger a_1 + |\nu|^2 a_2^\dagger a_2 + \mu^*\nu a_1^\dagger a_2 + \mu\nu^* a_2^\dagger a_1, \tag{90}$$

$$n_2 = |\nu|^2 a_1^\dagger a_1 + |\mu|^2 a_2^\dagger a_2 - \mu^*\nu a_1^\dagger a_2 - \mu\nu^* a_2^\dagger a_1. \tag{91}$$

#4717 - $15.00 US Received 1 July 2004; revised 30 September 2004; accepted 1 October 2004

For reference, one can deduce formula (91) from formula (90) by replacing the transfer functions μ and ν with $-\nu^*$ and μ^*, respectively.

First, suppose that the initial condition of the system is a number eigenstate with m_1 quanta of mode 1 and m_2 quanta of mode 2. Then it follows from Eqs. (90) and (91) that the output-number means

$$\langle n_1 \rangle = |\mu|^2 m_1 + |\nu|^2 m_2, \tag{92}$$

$$\langle n_2 \rangle = |\nu|^2 m_1 + |\mu|^2 m_2. \tag{93}$$

In contrast to the PA process, for the FC process there are no quantum contributions to the output numbers [10]. This result might lead one to conclude that FC is a noiseless process. However, such a conclusion is oversimplified.

It follows from Eq. (90) that the second-moment operator

$$\begin{aligned} n_1^2 = {} & (|\mu|^2 a_1^\dagger a_1 + |\nu|^2 a_2^\dagger a_2)^2 + (\mu^* \nu a_1^\dagger a_2 + \mu \nu^* a_2^\dagger a_1)^2 \\ & + (|\mu|^2 a_1^\dagger a_1 + |\nu|^2 a_2^\dagger a_2)(\mu^* \nu a_1^\dagger a_2 + \mu \nu^* a_2^\dagger a_1) \\ & + (\mu^* \nu a_1^\dagger a_2 + \mu \nu^* a_2^\dagger a_1)(|\mu|^2 a_1^\dagger a_1 + |\nu|^2 a_2^\dagger a_2). \end{aligned} \tag{94}$$

By proceeding as described after Eq. (79), one finds that the output-number variance

$$\langle \delta n_1^2 \rangle = |\mu|^2 |\nu|^2 (2 m_1 m_2 + m_1 + m_2). \tag{95}$$

The terms $m_1 + m_2$ are present in Eq. (95) because the creation and annihilation operators of modes 2 and 1, respectively, do not commute: Quantum noise is present at the output. It follows from the symmetry described after Eq. (91) that $\langle \delta n_2^2 \rangle = \langle \delta n_1^2 \rangle$. For the case in which mode 1 is a signal ($m_1 \neq 0$) and mode 2 is an idler ($m_2 = 0$), $\langle \delta n_j^2 \rangle = |\mu|^2 |\nu|^2 m_1$. The quantum contribution to the (common) output-number variance is equal to what one would predict classically by adding 1/2 of a noise photon to mode 2.

Second, suppose that the input signal (mode 1) has a Poisson number distribution with mean $\overline{m}_1$ and there is no input idler [Eq. (81)]. Then it follows from Eqs. (90) and (91) that

$$\langle n_1 \rangle = |\mu|^2 \overline{m}_1, \tag{96}$$

$$\langle n_2 \rangle = |\nu|^2 \overline{m}_1. \tag{97}$$

For the reasons stated before Eq. (84), it follows from Eqs. (94) and (95) that

$$\langle \delta n_1^2 \rangle = |\mu|^4 \overline{m}_1 + |\mu|^2 |\nu|^2 \overline{m}_1, \tag{98}$$

$$\langle \delta n_2^2 \rangle = |\nu|^4 \overline{m}_1 + |\mu|^2 |\nu|^2 \overline{m}_1. \tag{99}$$

The input uncertainty adds to the output uncertainties, but otherwise does not change the FC process. The SNRs and noise figures are defined for FC as they were defined for PA [before Eq. (86)]. Let $T = |\mu|^2$ denote the signal transmission. Then $|\nu|^2 = 1 - T$. It follows from Eqs. (96)–(99) that the FC noise-figures

$$F_1 = 1/T, \tag{100}$$

$$F_2 = 1/(1-T). \tag{101}$$

For the case in which $T = 1$, $F_1 = 1$ (0 dB), and for the case in which $T = 0$, $F_2 = 1$ (0 dB). For all other cases, in which $0 < T < 1$, $F_j > 1$. Equations (100) and (101) manifest the fact that the transmitted and frequency-converted images of a coherent state are also coherent states. The FC noise-figures are plotted as functions of distance in Fig. 3 for the case in which $\delta = 0$. [See Eq. (23).] The signal and idler noise-figures oscillate periodically between 1 and ∞. For $\delta \neq 0$ the signal noise-figure oscillates between 1 and $(\kappa^2 + \delta^2)/\delta^2 < \infty$ and the idler noise-figure oscillates between ∞ and $(\kappa^2 + \delta^2)/\kappa^2 > 1$.

#4717 - $15.00 US Received 1 July 2004; revised 30 September 2004; accepted 1 October 2004

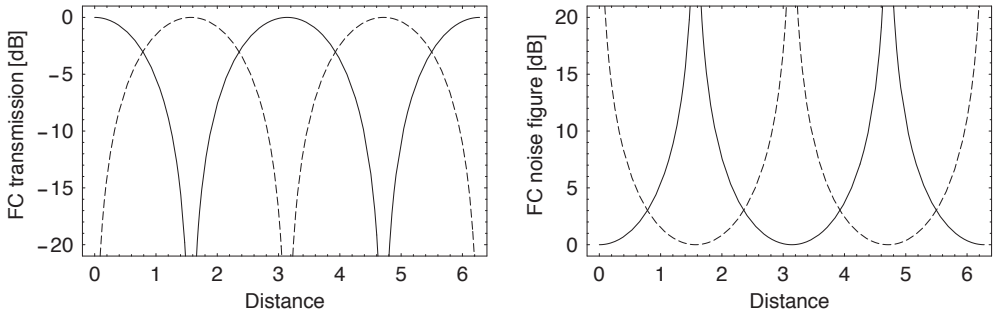

Fig. 3. Transmissions and noise figures of a two-mode frequency converter. The solid curves represent the signal, whereas the dashed curves represent the idler. Distance is normalized to the interaction length $[\gamma\varepsilon(P_1P_2)^{1/2}]^{-1}$.

7. Quantum many-mode processes

Equations (7)–(10) describe the classical version of a four-mode quantum process in which two creation operators (1 and 3) are coupled to two annihilation operators (2 and 4). As a prelude to the four-mode analysis, consider the simpler process in which a creation operator is only coupled to an annihilation operator and another creation operator. This three-mode process is governed by the matrix equation

$$B = MA, \tag{102}$$

where the input vector $A = (a_1^\dagger, a_2, a_3^\dagger)^T$, the output vector $B = (b_1^\dagger, b_2, b_3^\dagger)^T$ and the transfer matrix $M(z) = [\mu_{jk}(z)]$. As in Section 6, B also represents the intermediate states of the system at all positions within the parametric processor.

By evaluating the commutator $[b_1, b_1^\dagger]$ one finds that

$$|\mu_{11}|^2 - |\mu_{12}|^2 + |\mu_{13}|^2 = 1. \tag{103}$$

Notice that Eq. (103) reduces to Eq. (74) when $\mu_{13} = 0$, and reduces to Eq. (89) when $\mu_{12} = 0$. By evaluating the commutator $[b_2, b_2^\dagger]$ one finds that

$$-|\mu_{21}|^2 + |\mu_{22}|^2 - |\mu_{23}|^2 = 1. \tag{104}$$

Equation (104) also reduces to Eq. (74) when $\mu_{23} = 0$.

As in Section 6, the output-number operator $n_j = b_j^\dagger b_j$. It follows from Eq. (102) that

$$\begin{aligned} n_1 &= |\mu_{11}|^2 a_1^\dagger a_1 + |\mu_{12}|^2 a_2 a_2^\dagger + |\mu_{13}|^2 a_3^\dagger a_3 + \mu_{11}\mu_{12}^* a_1^\dagger a_2^\dagger + \mu_{12}\mu_{11}^* a_2 a_1 \\ &\quad + \mu_{12}\mu_{13}^* a_2 a_3 + \mu_{13}\mu_{12}^* a_3^\dagger a_2^\dagger + \mu_{13}\mu_{11}^* a_3^\dagger a_1 + \mu_{11}\mu_{13}^* a_1^\dagger a_3, \qquad (105) \\ n_2 &= |\mu_{21}|^2 a_1 a_1^\dagger + |\mu_{22}|^2 a_2^\dagger a_2 + |\mu_{23}|^2 a_3 a_3^\dagger + \mu_{21}^*\mu_{22} a_1 a_2 + \mu_{22}^*\mu_{21} a_2^\dagger a_1^\dagger \\ &\quad + \mu_{22}^*\mu_{23} a_2^\dagger a_3^\dagger + \mu_{23}^*\mu_{22} a_3 a_2 + \mu_{23}^*\mu_{21} a_3 a_1^\dagger + \mu_{21}^*\mu_{23} a_1 a_3^\dagger. \qquad (106) \end{aligned}$$

Here and subsequently, formulas for mode 3 are not stated explicitly because one can deduce them from the corresponding formulas for mode 1 by interchanging the subscripts 1 and 3.

If the input condition is a number eigenstate with m_j quanta of mode j, which is denoted by $|m_1, m_2, m_3\rangle$, the mean output number of mode j is $\langle m_1, m_2, m_3 | n_j | m_1, m_2, m_3\rangle$. Because different number states are orthogonal, it follows from Eqs. (105) and (106) that

$$\begin{aligned} \langle n_1\rangle &= |\mu_{11}|^2 m_1 + |\mu_{12}|^2 (m_2 + 1) + |\mu_{13}|^2 m_3, \qquad (107) \\ \langle n_2\rangle &= |\mu_{21}|^2 (m_1 + 1) + |\mu_{22}|^2 m_2 + |\mu_{23}|^2 (m_3 + 1). \qquad (108) \end{aligned}$$

#4717 - $15.00 US Received 1 July 2004; revised 30 September 2004; accepted 1 October 2004

Because the creation and annihilation operators of mode k do not commute, the output of mode $j \neq k$ includes quantum contributions of the form $1|\mu_{jk}|^2$. In the output of mode 1 (creation operator) there is a quantum contribution associated with mode 2 (annihilation operator), whereas in the output of mode 2 (annihilation operator) there are quantum contributions associated with modes 1 and 3 (creation operators): For each type of operator, the quantum contributions are associated with operators of the opposite type.

As in Section 6, the output-number variance $\langle \delta n_j^2 \rangle = \langle n_j^2 \rangle - \langle n_j \rangle^2$. One obtains formulas for the second-moment operators n_1^2 and n_2^2 by squaring the right sides of Eqs. (105) and (106), respectively. The first three terms on the right sides of Eqs. (105) and (106) contribute $\langle n_1 \rangle^2$ and $\langle n_2 \rangle^2$ to the variances of modes 1 and 2, which cancel the $-\langle n_1 \rangle^2$ and $-\langle n_2 \rangle^2$ terms in their definitions. Because different number states are orthogonal, only terms like $(\mu_{jk}\mu_{jl}^* a_k^\dagger a_l^\dagger + \mu_{jk}^* \mu_{jl} a_l a_k)^2$ contribute to the variances. It follows from these observations that

$$\begin{aligned} \langle \delta n_1^2 \rangle &= |\mu_{11}\mu_{12}|^2(2m_1m_2 + m_1 + m_2 + 1) \\ &\quad + |\mu_{12}\mu_{13}|^2(2m_2m_3 + m_2 + m_3 + 1) \\ &\quad + |\mu_{13}\mu_{11}|^2(2m_3m_1 + m_3 + m_1), \qquad (109) \\ \langle \delta n_2^2 \rangle &= |\mu_{21}\mu_{22}|^2(2m_1m_2 + m_1 + m_2 + 1) \\ &\quad + |\mu_{22}\mu_{23}|^2(2m_2m_3 + m_2 + m_3 + 1) \\ &\quad + |\mu_{23}\mu_{21}|^2(2m_3m_1 + m_3 + m_1). \qquad (110) \end{aligned}$$

Equations (109) and (110) contain terms associated with all possible combinations of modes k and $l \neq k$. If the operators of modes k and l are of the same type the associated term contains the factor $(m_k m_l + m_k + m_l)$, whereas if the operators are of opposite types the associated term contains the factor $(m_k m_l + m_k + m_l + 1)$. It is clear from Eqs. (109) and (110) that the price one pays for additional coupling (and higher gain) is additional quantum noise.

If the input signal (mode 1) has a Poisson number distribution with mean $\overline{m}_1$ and there are no input idlers [Eq. (81), with $|m_1,0\rangle$ replaced with $|m_1,0,0\rangle$], the output-number means

$$\begin{aligned} \langle n_1 \rangle &= |\mu_{11}|^2 \overline{m}_1 + |\mu_{12}|^2, \qquad (111) \\ \langle n_2 \rangle &= |\mu_{21}|^2 (\overline{m}_1 + 1) + |\mu_{23}|^2. \qquad (112) \end{aligned}$$

A Poisson distribution with mean $\overline{m}$ also has variance $\overline{m}$. This uncertainty adds $|\mu_{11}|^4 \overline{m}_1$ and $|\mu_{21}|^4 \overline{m}_1$ to the squares of the first terms in Eqs. (105) and (106), respectively. The contributions of terms like $(\mu_{jk}\mu_{jl}^* a_k^\dagger a_l^\dagger + \mu_{jk}^* \mu_{jl} a_l a_k)^2$ are unchanged. Although $\langle m_1,0,0|n_1,0,0\rangle \neq 0$ for a Poisson state, the other terms in the second-moment operators contain unbalanced powers of $a_2^{(\dagger)}$ or $a_3^{(\dagger)}$, so the associated inner products remain zero. Hence, the output-number variances

$$\begin{aligned} \langle \delta n_1^2 \rangle &= |\mu_{11}|^4 \overline{m}_1 + |\mu_{11}\mu_{12}|^2 (\overline{m}_1 + 1) + |\mu_{12}\mu_{13}|^2 + |\mu_{13}\mu_{11}|^2 \overline{m}_1, \qquad (113) \\ \langle \delta n_2^2 \rangle &= |\mu_{21}|^4 \overline{m}_1 + |\mu_{21}\mu_{22}|^2 (\overline{m}_1 + 1) + |\mu_{22}\mu_{23}|^2 + |\mu_{23}\mu_{21}|^2 \overline{m}_1. \qquad (114) \end{aligned}$$

By comparing Eqs. (113) and (114) with the $m_2 = m_3 = 0$ limit of Eqs. (109) and (110), one finds that the input uncertainty adds to the output uncertainties, but does not otherwise change the three-mode process.

As in Section 6, the SNR of mode j is defined as $\langle n_j \rangle / \langle \delta n_j^2 \rangle$ and the noise figure of mode j is defined as the input SNR of mode 1 (which is $\overline{m}_1$) divided by the output SNR of mode j. It follows from Eqs. (111)–(114) that the noise figures

$$F_1 = \frac{\overline{m}_1 [|\mu_{11}|^4 \overline{m}_1 + |\mu_{11}\mu_{12}|^2 (\overline{m}_1 + 1) + |\mu_{12}\mu_{13}|^2 + |\mu_{13}\mu_{11}|^2 \overline{m}_1]}{[|\mu_{11}|^2 \overline{m}_1 + |\mu_{12}|^2]^2}, \qquad (115)$$

#4717 - $15.00 US Received 1 July 2004; revised 30 September 2004; accepted 1 October 2004

$$F_2 = \frac{\overline{m}_1[|\mu_{21}|^4\overline{m}_1 + |\mu_{21}\mu_{22}|^2(\overline{m}_1+1) + |\mu_{22}\mu_{23}|^2 + |\mu_{23}\mu_{21}|^2\overline{m}_1]}{[|\mu_{21}|^2(\overline{m}_1+1) + |\mu_{23}|^2]^2}. \tag{116}$$

For reference, one can deduce the noise figure for mode 3 from Eq. (115) by replacing μ_{1k} with μ_{3k}. Notice that Eqs. (115) and (116) reduce to Eqs. (86) and (87), respectively, when $\mu_{13} = \mu_{23} = 0$. Equation (115) and its analog for mode 3 reduce to Eqs. (100) and (101), respectively, when $\mu_{12} = \mu_{32} = 0$: The two-mode results are special cases of the three-mode results. For the common limit in which $\overline{m}_1 \gg 1$,

$$F_1 \approx 1 + (|\mu_{12}|^2 + |\mu_{13}|^2)/|\mu_{11}|^2, \tag{117}$$

$$F_2 \approx 1 + (|\mu_{22}|^2 + |\mu_{23}|^2)/|\mu_{21}|^2. \tag{118}$$

For reference, one can deduce results for the interaction of an annihilation operator with a creation operator and another annihilation operator by taking the hermitian conjugate of the preceding results.

The preceding analysis of the three-mode process shows clearly how quantum contributions to the output-number means and variances accumulate. Not only can results be inferred for four-mode processes, they can also be inferred for processes with arbitrary numbers of interacting modes. It follows from the commutator conservation equations that

$$\sum_k |\mu_{jk}|^2 s_{jk} = 1, \tag{119}$$

where $s_{jk} = 1$ if operators j and k are of the same type (both creation or both annihilation), and $s_{jk} = -1$ if they are of different types (one creation and one annihilation).

If the initial condition of the system is a number eigenstate with m_j quanta of mode j, the output-number means

$$\langle n_j \rangle = \sum_k |\mu_{jk}|^2 (m_k + \sigma_{jk}), \tag{120}$$

where $\sigma_{jk} = 0$ if operators j and k are of the same type and $\sigma_{jk} = 1$ if operators j and k are of opposite types. The output-number variances

$$\langle \delta n_j^2 \rangle = \sum_{k,l>k} |\mu_{jk}\mu_{jl}|^2 (2m_k m_l + m_k + m_l + \sigma_{kl}), \tag{121}$$

where the summation is made over both subscripts (k and l). Notice that the number of terms that contribute to each variance is (approximately) equal to half the square of the number of modes.

If mode i is the signal, and has a Poisson number distribution with mean $\overline{m}_i$, and the other modes are idlers, the output-number means

$$\langle n_j \rangle = |\mu_{ji}|^2 \overline{m}_i + \sum_k |\mu_{jk}|^2 \sigma_{jk} \tag{122}$$

and the output-number variances

$$\langle \delta n_j^2 \rangle = |\mu_{ji}|^4 \overline{m}_i + \sum_{k \neq i} |\mu_{ji}\mu_{jk}|^2 \overline{m}_i + \sum_{k,l>k} |\mu_{jk}\mu_{jl}|^2 \sigma_{kl}, \tag{123}$$

where the second summation is made over both subscripts. It follows from Eqs. (122) and (123) that the noise figures

$$F_j = \frac{\overline{m}_i \left(|\mu_{ji}|^4 \overline{m}_i + \sum_{k \neq i} |\mu_{ji}\mu_{jk}|^2 \overline{m}_i + \sum_{k,l>k} |\mu_{jk}\mu_{jl}|^2 \sigma_{kl} \right)}{\left(|\mu_{ji}|^2 \overline{m}_i + \sum_k |\mu_{jk}|^2 \sigma_{jk} \right)^2}. \tag{124}$$

#4717 - $15.00 US Received 1 July 2004; revised 30 September 2004; accepted 1 October 2004

For the common limit in which $\overline{m}_i \gg \sigma_{jk}$,

$$F_j \approx 1 + \sum_{k \neq i} |\mu_{jk}|^2 / |\mu_{ji}|^2. \tag{125}$$

Despite the complexity of the process, the final result is simple. The number of contributions to each noise figure is equal to the number of modes. The first contribution can be traced to the photon-number uncertainty of the (coherent) signal, whereas the other contributions can be traced to the photon-number uncertainties of the (generated) idlers. For brevity, we refer to both types of uncertainty as vacuum fluctuations.

8. Discussion

Equation (125) is valid for an arbitrary number of modes, provided that only the signal mode has a nonzero input photon-number. In this section the consequences of Eq. (125) are discussed for PA driven by two pumps, which is a four-mode (FM) process. (The pump modes are excluded from this count, because they are considered to be classical fields.)

Consider the second example of Section 4, in which the mode powers grow quadratically with distance [Eq. (35)], and suppose that the $1-$ mode is the signal. Then, in the long-distance limit ($\gamma P z \gg 1$), Eq. (125) implies that

$$F_{1\pm} = 2 + 2\varepsilon^2, \tag{126}$$

$$F_{2\pm} = 2 + 2/\varepsilon^2. \tag{127}$$

For co-polarized pumps $\varepsilon = 2$, so $F_{1\pm} = 10$ (10 dB) and $F_{2\pm} = 2.5$ (4.0 dB): The noise figures of the signal and $1+$ idler are too high for these modes to be useful, but the noise figures of the $2-$ and $2+$ idlers are low (and the $2+$ idler is a phase-conjugated image of the signal). In contrast, for cross-polarized pumps in a fiber with constant birefringence $\varepsilon = 2/3$, so $F_{1\pm} = 2.9$ (4.6 dB) and $F_{2\pm} = 6.5$ (8.1 dB): The noise figures of the $2-$ and $2+$ idlers are too high for these modes to be useful, but the noise figures of the signal and $1+$ idler are low (and the $1+$ idler is a phase-conjugated image of the signal). For cross-polarized pumps in a fiber with random birefringence $\varepsilon = 1$, so $F_{1\pm} = 4$ (6 dB) and $F_{2\pm} = 4$ (6 dB). The signal and idler noise-figures are plotted as functions of distance in Figs. 4–6. In all three cases the signal noise-figure increases monotonically and the idler noise-figures decrease monotonically.

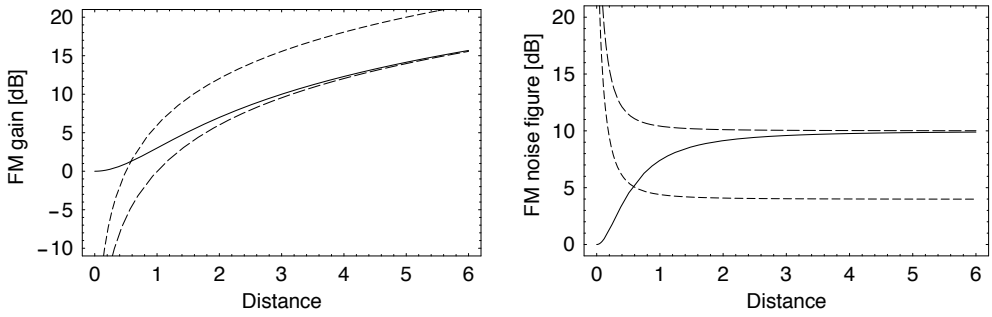

Fig. 4. Gains and noise figures of a four-mode process with quadratic gain, for co-polarized pumps ($\varepsilon = 2$). The solid and long-dashed curves represent the $1-$ signal and $1+$ idler, respectively, and the medium-dashed curves represent the $2-$ and $2+$ idlers. Distance is normalized to the characteristic length $(\gamma P)^{-1}$.

#4717 - $15.00 US Received 1 July 2004; revised 30 September 2004; accepted 1 October 2004

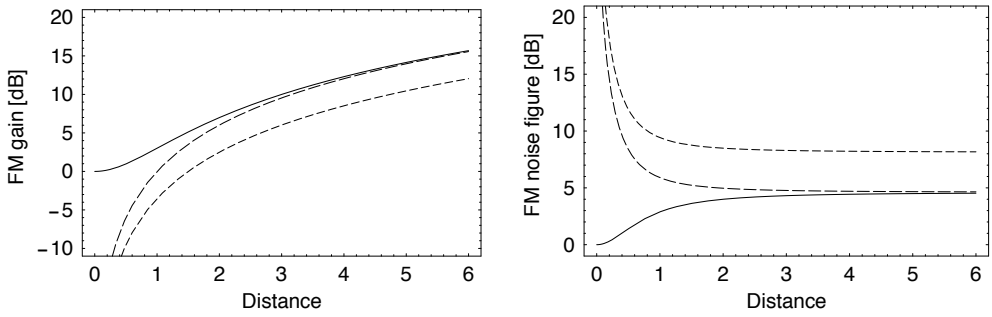

Fig. 5. Gains and noise figures of a four-mode process with quadratic gain, for cross-polarized pumps in a fiber with constant birefringence ($\varepsilon = 2/3$). The solid and long-dashed curves represent the $1-$ signal and $1+$ idler, respectively, and the medium-dashed curves represent the $2-$ and $2+$ idlers. Distance is normalized to the characteristic length $(\gamma P)^{-1}$.

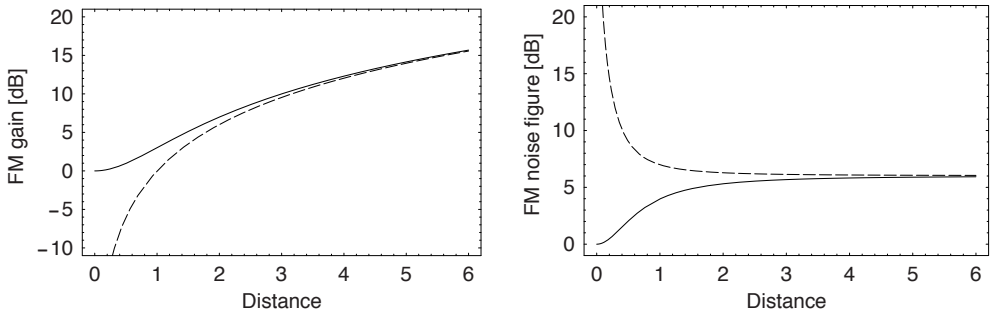

Fig. 6. Gains and noise figures of a four-mode process with quadratic gain, for cross-polarized pumps in a fiber with random birefringence ($\varepsilon = 1$). The solid curve represents the $1-$ signal, and the long-dashed curves represent the $1+$, $2-$ and $2+$ idlers. Distance is normalized to the characteristic length $(\gamma P)^{-1}$.

Now consider the third example of Section 4, in which the mode powers grow exponentially with distance [Eq. (36)], at the rate $\kappa_+ = 2\gamma(1+\varepsilon)P$. Then, in the long-distance limit ($\kappa_+ z \gg 1$) all elements of the transfer matrix have the same modulus. Hence,

$$F_{1\pm} = F_{2\pm} = 4. \tag{128}$$

It should come as no surprise that all four modes contribute equally to the noise figures, because the maximal-gain condition $\beta_e = -\gamma(1+\varepsilon)P$ ensures that all four modes are driven resonantly and, hence, participate equally in the instability. The signal and idler noise-figures are plotted as functions of distance in Fig. 7 for the case in which $\varepsilon = 1$. The signal and idler noise-figures do not evolve monotonically because the recessive wavenumber k_- is real: The four-mode process exhibits characteristics of both constituent two-mode processes. (See Figs. 2 and 3.)

The preceding examples illustrate the general guideline that noise figures increase in direct proportion to the number of modes involved in the mixing process. This guideline might lead one to conclude that many-mode parametric devices are impractical. Fortunately, such a conclusion is unnecessarily pessimistic. It is possible to tune the pump frequencies in such a way that all four mode powers are comparable [4, 23, 24], in which case the output noise should be monitored carefully. However, if the pump frequencies are tuned to maximize the PA band-

#4717 - $15.00 US Received 1 July 2004; revised 30 September 2004; accepted 1 October 2004

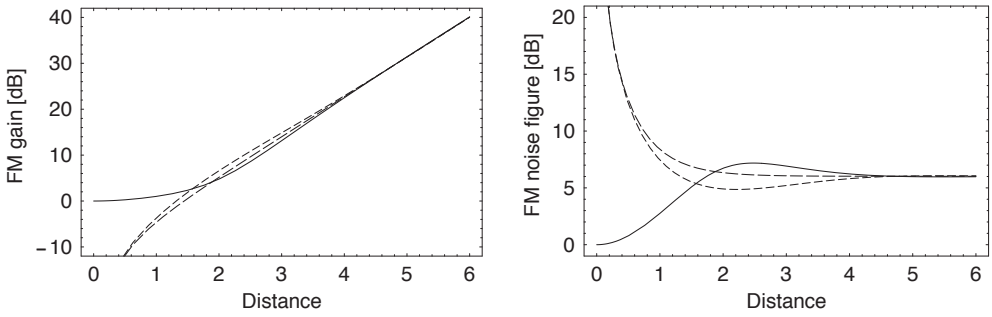

Fig. 7. Gains and noise figures of a four-mode process with exponential gain, for cross-polarized pumps in a fiber with random birefringence ($\varepsilon = 1$). The solid curves represent the $1-$ signal, the long-dashed curves represent the $1+$ and $2+$ idlers, and the medium-dashed curves represent the $2-$ idler. Distance is normalized to the gain length $(2\gamma P)^{-1}$.

width the powers of the signal and primary (PC) idler are usually (at least) 10-dB higher than the powers of the secondary idlers [3, 4, 25], and if the pump frequencies are tuned to maximize the FC bandwidth the powers of the signal and primary (BS) idler are usually (about) 10-dB higher than the powers of the secondary idlers [7]. These (simulated and measured) differences in mode powers reflect differences in the same transfer functions that determine the noise figures: For the stated applications, coupling to extra modes (secondary idlers) should only increase the signal and primary-idler noise-figures slightly.

To validate the preceding conclusion the transfer functions μ_{jk} were determined by solving Eqs. (7)–(10) numerically, and the noise figures were determined from these transfer functions and Eq. (125). The signal and idler noise-figures are plotted as functions of frequency in Fig. 8, for parameters that are representative of current experiments: The third-order dispersion

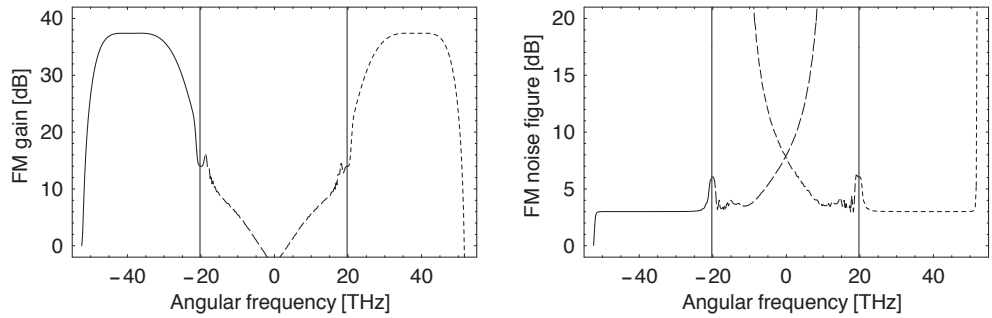

Fig. 8. Gains and noise figures of a four-mode process driven by cross-polarized pumps in a fiber with random birefringence ($\varepsilon = 1$). The solid curves represent the $1-$ signal, and the long-, medium- and short-dashed curves represent the $1+$, $2-$ and $2+$ idlers, respectively. Frequencies are measured relative to the zero-dispersion frequency of the fiber. The vertical lines denote the pump frequencies.

coefficient $\beta^{(3)}(\omega_0) = 0.1$ ps^3/Km and the fourth-order dispersion coefficient $\beta^{(4)}(\omega_0) = 10^{-4}$ ps^4/Km, where the reference frequency ω_0 is the zero-dispersion frequency (ZDF) of the fiber. The nonlinearity coefficient $\gamma = 10$/Km-W, the fiber length $l = 1.0$ Km and the common pump power $P = 0.5$ W. A good PA can amplify many frequency-diverse signals simultaneously [25]. For the aforementioned parameters, broad-bandwidth gain occurs when the pump frequencies

#4717 - $15.00 US Received 1 July 2004; revised 30 September 2004; accepted 1 October 2004

$\omega_1 \approx -20.3$ and $\omega_2 \approx 19.7$ THz are approximately equidistant from the ZDF. (We use THz as an informal abbreviation for Trad/s.) For signal ($1-$) frequencies between -50 and -25 THz, the primary-idler ($2+$) gain is comparable to the signal gain, both of which are at least 25-dB higher than the secondary-idler ($1+$ and $2-$) gains. The associated signal and primary-idler noise-figures are both about 3 dB, as predicted. The secondary-idler noise-figures are much higher. Near the outer edge of the gain band ($\omega_{1-} \approx -52$ THz) the signal gain decreases to zero. The associated signal noise-figure decreases to zero, whereas the associated primary-idler noise-figure increases to infinity ($\omega_{2+} \approx 52$ THz). This behavior is analogous to the low-gain behavior exhibited in Fig. 6(b). Near the inner edge of the gain band ($\omega_{1-} \approx -21$ THz) the gains of all four modes are comparable. In this region the signal and idler noise-figures are all about 6 dB. This behavior is analogous to the high-gain behavior exhibited in Fig. 6(b).

The results are similar if one of the other modes is the signal. Noise-figures are plotted as functions of frequency in Fig. 9, for the case in which the $1+$ mode is the signal. For this case,

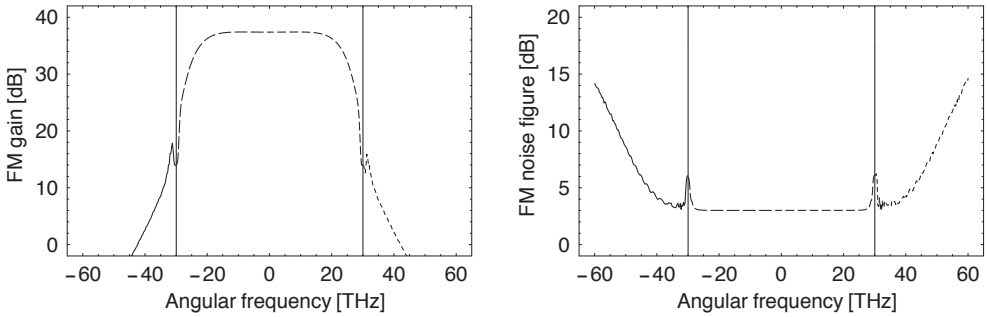

Fig. 9. Gains and noise figures of a four-mode process driven by cross-polarized pumps in a fiber with random birefringence ($\varepsilon = 1$). The long-dashed curves represent the $1+$ signal, and the solid, medium- and short-dashed curves represent the $1-$, $2-$ and $2+$ idlers, respectively. Frequencies are measured relative to the zero-dispersion frequency of the fiber. The vertical lines denote the pump frequencies.

broad-bandwidth gain occurs when the pump frequencies $\omega_1 \approx -30.0$ and $\omega_2 \approx 30.0$ THz (and the other system parameters are the same as those associated with Fig. 8). For signal frequencies between -25 and 0 THz, the primary-idler ($2-$) gain is comparable to the signal gain, both of which are at least 25-dB higher than the secondary-idler ($2+$ and $1-$) gains. The associated signal and primary-idler noise-figures are both about 3 dB, as predicted. Near the outer edge of the gain band ($\omega_{1+} \approx -29$ THz) the gain of all four modes is comparable, and the signal and idler noise-figures are all about 6 dB. This behavior is analogous to the high-gain behavior exhibited in Fig. 6(b).

Not only can parametric devices provide PA, they can also provide tunable FC [7]. This function is made possible by BS. For example, consider the BS process associated with the frequency-matching condition $\omega_{1+} + \omega_2 = \omega_1 + \omega_{2+}$. In the standard FC scheme the signal frequency (ω_{1+}) and one of the pump frequencies (ω_2) are fixed. By varying the frequency of the other pump (ω_1), one can vary the primary-idler frequency (ω_{2+}). Because BS is driven by two pumps, secondary ($1-$ and $2-$) idlers are also produced. The signal and idler noise-figures are plotted as functions of frequency in Fig. 10. The fiber dispersion and nonlinearity coefficients, and the common pump power, are the same as those associated with Fig. 8. The fiber length $l = 0.52$ Km was chosen so that the BS wavenumber $k = \pi/2$, for the ideal case in which $\delta = 0$. This condition enables a complete photon-flux transfer from the signal to the primary idler, as implied by Eq. (23). For these parameters, broad-bandwidth FC occurs

#4717 - $15.00 US Received 1 July 2004; revised 30 September 2004; accepted 1 October 2004

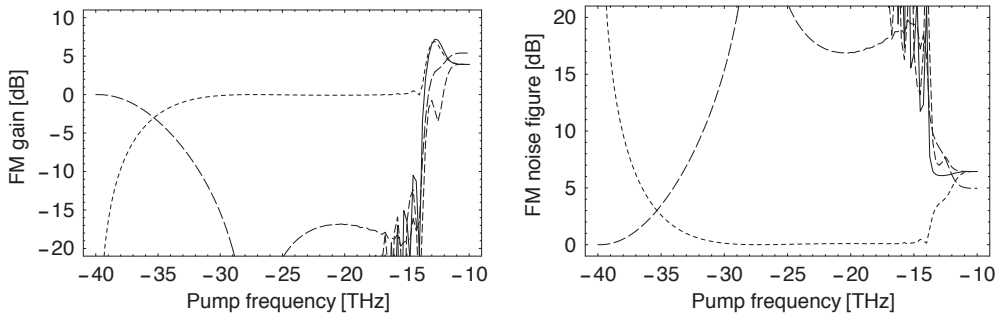

Fig. 10. Transmissions and noise figures of a four-mode process driven by cross-polarized pumps in a fiber with random birefringence ($\varepsilon = 1$), plotted as functions of the pump frequency ω_1. The long-dashed curves represent the $1+$ signal, and the solid, medium- and short-dashed curves represent the $1-$, $2-$ and $2+$ idlers, respectively. Frequencies are measured relative to the zero-dispersion frequency of the fiber.

when the signal frequency $\omega_2 = -10.1$ THz and the higher pump-frequency $\omega_2 = 9.9$ THz are approximately equidistant from the ZDF. As the lower pump-frequency ω_1 varies from (about) -10 to -40 THz, the primary-idler frequency $\omega_{2+} = \omega_{1+} + \omega_2 - \omega_1$ varies from 10 to 40 THz, and the secondary-idler frequencies $\omega_{1-} = 2\omega_1 - \omega_{1+}$ and $\omega_{2-} = \omega_1 + \omega_2 - \omega_{1+}$ vary from -10 to -70 THz and from 10 to -20 THz, respectively. For pump frequencies near the signal frequency ($\omega_1 \approx -10$ THz) the effects of dispersion are weak and all four modes participate strongly in the interaction. (The gains displayed in Fig. 10(a) are lower than those displayed in Fig. 6(a) because the fiber is shorter.) Consequently, the signal and idler noise-figures are all about 6 dB. This behavior is analogous to the moderate-gain behavior exhibited in Fig. 6(b). As the difference between the pump and signal frequencies increases, the secondary-idler gains decrease. For most pump frequencies between -35 and -15 THz the signal transmission is less than -15 dB and the primary-idler transmission is about 0 dB: The photon-flux transfer is nearly complete. Throughout this frequency range the primary-idler noise-figure is close to 0 dB and the signal noise-figure is higher than 15 dB.

For reference, the noise properties of erbium and Raman amplifiers are discussed in [26] and [27], respectively. Other papers on the noise properties of linear amplifiers are listed in [15] and [16].

9. Summary

In a parametric device driven by one pump wave, the signal sideband is coupled to an idler sideband, which is a frequency-converted (FC) image of the signal. Such a device is based on a two-sideband (TS) interaction. Depending on the way in which the device is configured, the signal might (not) be amplified and the idler might (not) be a phase-conjugated (PC) image of the signal. The quantum noise properties of one-pump devices are known [12].

In a parametric device driven by two pump waves the signal sideband is coupled to three idler sidebands, all of which are FC images of the signal, and two of which are PC images of the signal. A typical two-pump device provides more amplification, over a broader frequency-bandwidth, than a typical one-pump device. However, if the two-pump device is to be useful, the signal must be amplified, and the PC and FC idlers must be produced, with minimal noise.

In this paper the quantum noise properties of two-sideband (TS) devices were reviewed. Formulas were derived for the signal and idler noise-figures of (unstable) parametric amplifiers (PAs) and (stable) FCs [Eqs. (86) and (87), and Eqs. (100) and (101), respectively]. The noise

#4717 - $15.00 US Received 1 July 2004; revised 30 September 2004; accepted 1 October 2004

figures of good (one-pump) PAs are about 3 dB, whereas the noise figures of good (one-pump) FCs can be as low as 0 dB. However, the lower noise-figures of the latter devices are offset by the absence of gain.

The mathematical method applied to, and the physical insight gained from, the study of these TS devices were used to derive formulas for the signal and idler noise-figures of devices with arbitrary numbers of interacting sidebands [Eqs. (124) and (125)]. Because noise is produced by the amplification or combination of the vacuum fluctuations associated with each sideband, the noise levels increase in proportion to the number of sidebands that interact strongly. The general results were applied to the study of two-pump devices, which are based on the aforementioned four-sideband (FS) interaction. The noise figure of a (two-pump) fiber PA depends on the fiber type and pump polarizations. We considered co- and cross-polarized pumps in fibers with constant and random birefringence. If the pump frequencies are tuned to equalize the signal and idler gains, the noise figures range from 4 dB to 10 dB [Eqs. (126)–(128)]. However, if the pump frequencies are tuned to maximize the frequency bandwidth of the FS interaction, the signal and primary-idler noise-figures are only slightly higher than the noise figures associated with the limiting TS interactions: PA with signal and primary-idler noise-figures of about 3 dB, and FC with a primary-idler noise-figure of about 0 dB, are possible.

Acknowledgments

The research of SR and MGR was supported by the National Science Foundation, under contracts ECS-0406379 and ECS-0323141, respectively.

Appendix A: Special solutions of the four-sideband equations

As stated in Section 4, Eqs. (7)–(10) can be rewritten in the matrix form

$$d_z B = LB, \tag{129}$$

where $B = (B_{1-}^*, B_{1+}, B_{2-}^*, B_{2+})^T$ and L is a constant matrix. In the first example of Section 4, the nonlinear contributions to L, which are of order γP, are much smaller than the dispersive contributions, which are of order $\beta_{j\pm}$. Hence, one can solve Eq. (129) by using the multiple-scale perturbation method [28].

Let $\nu \ll 1$ be the order parameter. [We use ν only for the purpose of book-keeping: Eq. (129) is not rewritten in dimensionless form.] Furthermore, let $B = B^{(0)} + \nu B^{(1)}$, $z_0 = z$, $z_1 = \nu z$ and $d/dz = d/dz_0 + \nu d/dz_1$. Then, by making these substitutions in Eq. (129) and collecting terms of like order, one finds that

$$d_{z_0} B^{(0)} - L^{(0)} B^{(0)} = 0, \tag{130}$$

$$d_{z_0} B^{(1)} - L^{(0)} B^{(1)} = -d_{z_1} B^{(0)} + L^{(1)} B^{(0)}, \tag{131}$$

where $L^{(0)} = \mathrm{diag}(-i\beta_{1-}, i\beta_{1+}, -i\beta_{2-}, i\beta_{2+})$ and $L^{(1)} = \left[l_{jk}^{(1)}\right]$ is the matrix of nonlinear coefficients (all of which are proportional to γ). It follows from Eq. (130) that

$$B_j^{(0)}(z_0) = C_j^{(0)} \exp\left[\lambda_j^{(0)} z_0\right], \tag{132}$$

where $\lambda_j^{(0)}$ is an eigenvalue of $L^{(0)}$ and j = 1–4. By substituting the zeroth-order solution (132) into Eq. (131), one finds that

$$d_{z_0} B_j^{(1)} - \lambda_j^{(0)} B_j^{(1)} = -d_{z_1} C_j^{(0)} \exp\left[\lambda_j^{(0)} z_0\right] + \sum_k l_{jk}^{(1)} C_k^{(0)} \exp\left[\lambda_k^{(0)} z_0\right]. \tag{133}$$

#4717 - $15.00 US Received 1 July 2004; revised 30 September 2004; accepted 1 October 2004

$B^{(1)}$ will contain (secular) terms that grow as z_0 unless

$$d_{z_1} C_j^{(0)} = l_{jj}^{(1)} C_j^{(0)}, \tag{134}$$

from which it follows that

$$C_j^{(0)}(z_1) = C_j^{(0)}(0) \exp\left[l_{jj}^{(1)} z_1\right]. \tag{135}$$

It follows from Eqs. (133) and (134) that the (nonsecular) first-order solution

$$B_j^{(1)}(z_0) = \sum_{k \neq j} l_{jk}^{(1)} C_k^{(0)} \frac{\exp\left[\lambda_k^{(0)} z_0\right] - \exp\left[\lambda_j^{(0)} z_0\right]}{\lambda_k^{(0)} - \lambda_j^{(0)}}. \tag{136}$$

By combining solutions (132), (135) and (136), and removing the book-keeping parameter, one obtains solution (32). This method of solution also works for the general case in which $L^{(0)}$ is not diagonal. For reference, if one were to renormalize the zeroth-order equations by defining $\overline{\lambda}_j^{(0)} = \lambda_j^{(0)} + l_{jj}^{(1)}$, the first-order equations would not contain secularity-producing terms and one could use a regular perturbation method to solve Eq. (129).

The solution of Eq. (129) can be written in the form

$$B(z) = M(z) B(0), \tag{137}$$

where the transfer matrix $M(z) = \exp(Lz) = \sum_n (Lz)^n / n!$. In the second example of Section 4 the modulation frequency is low ($\omega \approx 0$), $L^n \approx 0$ for $n \geq 2$ and

$$M(z) \approx 1 + Lz. \tag{138}$$

Formula (138) is valid for arbitrary pump powers.

Let β_{je} and β_{jo} denote the even and odd terms in the Taylor expansions of $\beta_{j\pm} = \beta_j(\pm\omega)$. In the third example of Section 4 $\beta_{1e} \approx \beta_{2e} = \beta_e$, $\beta_{1o} \approx \beta_{2o} = \beta_o$ and $P_1 = P_2 = P$. Let $B_{j\pm}^{(*)} = C_{j\pm}^{(*)} \exp(i\beta_o z)$. Then the transformed amplitudes satisfy Eqs. (7)–(10), with $\beta_{j\pm}$ replaced by β_e.

Let $G_j = C_{j+} + C_{j-}^*$ and $H_j = C_{j+} - C_{j-}^*$. Then the transformed versions of Eqs. (7)–(10) can be rewritten in the form

$$d_z G_j = i\beta_e H_j, \tag{139}$$

$$d_z H_j = i(\beta_e + 2\gamma P) G_j + i2\gamma\varepsilon P G_k, \tag{140}$$

where $j = 1$ or 2 and $k \neq j$. By combining Eqs. (139) and (140), one finds that

$$[d_{zz}^2 + \beta_e(\beta_e + 2\gamma P)] G_1 + 2\beta_e \gamma\varepsilon P G_2 = 0, \tag{141}$$

$$2\beta_e \gamma\varepsilon P G_1 + [d_{zz}^2 + \beta_e(\beta_e + 2\gamma P)] G_2 = 0. \tag{142}$$

It follows from Eqs. (141) and (142) that the FS wavenumbers

$$k_\pm^2 = \beta_e[\beta_e + 2\gamma(1 \pm \varepsilon)P]. \tag{143}$$

Let $C = (C_{1-}^*, C_{1+}, C_{2-}^*, C_{2+})^T$ and suppose that $C(0) = (1,0,0,0)^T$. Then $G_1(0) = 1$, $H_1(0) = -1$ and $G_2(0) = H_2(0) = 0$. Conversely, suppose that $C(0) = (0,1,0,0)^T$. Then $G_1(0) = 1$, $H_1(0) = 1$ and $G_2(0) = H_2(0) = 0$. One can consider both cases simultaneously by defining $H_1(0) = \sigma$, where $\sigma = \mp 1$, respectively. It is not difficult to show that

$$G_1 = \frac{1}{2}\cos(k_+ z) + \frac{i\sigma\beta_e}{2k_+}\sin(k_+ z) + \frac{1}{2}\cos(k_- z) + \frac{i\sigma\beta_e}{2k_-}\sin(k_- z), \tag{144}$$

#4717 - $15.00 US
Received 1 July 2004; revised 30 September 2004; accepted 1 October 2004

$$H_1 = \frac{\sigma}{2}\cos(k_+z) + \frac{ik_+}{2\beta_e}\sin(k_+z) + \frac{\sigma}{2}\cos(k_-z) + \frac{ik_-}{2\beta_e}\sin(k_-z), \quad (145)$$

$$G_2 = \frac{1}{2}\cos(k_+z) + \frac{i\sigma\beta_e}{2k_+}\sin(k_+z) - \frac{1}{2}\cos(k_-z) - \frac{i\sigma\beta_e}{2k_-}\sin(k_-z), \quad (146)$$

$$H_2 = \frac{\sigma}{2}\cos(k_+z) + \frac{ik_+}{2\beta_e}\sin(k_+z) - \frac{\sigma}{2}\cos(k_-z) - \frac{ik_-}{2\beta_e}\sin(k_-z). \quad (147)$$

It follows from Eqs. (144)–(147), and the inversion formulas $C_{j+} = (G_j + H_j)/2$ and $C^*_{j-} = (G_j - H_j)/2$, that

$$C^*_{1-} = \frac{1-\sigma}{4}\cos(k_+z) + \frac{i}{4}\left(\frac{\sigma\beta_e}{k_+} - \frac{k_+}{\beta_e}\right)\sin(k_+z) + \frac{1-\sigma}{4}\cos(k_-z) + \frac{i}{4}\left(\frac{\sigma\beta_e}{k_-} - \frac{k_-}{\beta_e}\right)\sin(k_-z), \quad (148)$$

$$C_{1+} = \frac{1+\sigma}{4}\cos(k_+z) + \frac{i}{4}\left(\frac{\sigma\beta_e}{k_+} + \frac{k_+}{\beta_e}\right)\sin(k_+z) + \frac{1+\sigma}{4}\cos(k_-z) + \frac{i}{4}\left(\frac{\sigma\beta_e}{k_-} + \frac{k_-}{\beta_e}\right)\sin(k_-z), \quad (149)$$

$$C^*_{2-} = \frac{1-\sigma}{4}\cos(k_+z) + \frac{i}{4}\left(\frac{\sigma\beta_e}{k_+} - \frac{k_+}{\beta_e}\right)\sin(k_+z) - \frac{1-\sigma}{4}\cos(k_-z) - \frac{i}{4}\left(\frac{\sigma\beta_e}{k_-} - \frac{k_-}{\beta_e}\right)\sin(k_-z), \quad (150)$$

$$C_{2+} = \frac{1+\sigma}{4}\cos(k_+z) + \frac{i}{4}\left(\frac{\sigma\beta_e}{k_+} + \frac{k_+}{\beta_e}\right)\sin(k_+z) - \frac{1+\sigma}{4}\cos(k_-z) - \frac{i}{4}\left(\frac{\sigma\beta_e}{k_-} + \frac{k_-}{\beta_e}\right)\sin(k_-z). \quad (151)$$

Formulas (148)–(151) define the first and second columns of the transfer matrix. One can deduce formulas for the elements of the third and fourth columns by interchanging the subscripts 1 and 2.

It follows from Eq. (143) that the growth rate (imaginary root of the characteristic equation) attains its maximal value $\kappa_+ = \gamma(1+\varepsilon)P$ when $\beta_e = -\gamma(1+\varepsilon)P$. For this value of β_e the other root k_- is real (because $\varepsilon \geq 1/3$ for the fibers under consideration). Equation (36) follows from Eqs. (148)–(151), in the long-distance limit ($\kappa_+ z \gg 1$).

It is not difficult to extend the preceding analysis to cases in which $\beta_{1e} \neq \beta_{2e}$ and $P_1 \neq P_2$, some of which are relevant to broad-bandwidth PA. In such cases Eqs. (7)–(10) can be rewritten in the form

$$d_z G_j = i\beta_{je} H_j, \quad (152)$$

$$d_z H_j = i(\beta_{je} + 2\gamma P_j)G_j + i2\gamma\varepsilon(P_j P_k)^{1/2} G_k, \quad (153)$$

where $j = 1$ or 2 and $k \neq j$. By combining Eqs. (152) and (153), one finds that

$$[d_{zz}^2 + \beta_{1e}(\beta_{1e} + 2\gamma P_1)]G_1 + 2\beta_{1e}\gamma\varepsilon(P_1P_2)^{1/2}G_2 = 0, \quad (154)$$

$$2\beta_{2e}\gamma\varepsilon(P_1P_2)^{1/2}G_1 + [d_{zz}^2 + \beta_{2e}(\beta_{2e} + 2\gamma P_2)]G_2 = 0. \quad (155)$$

It follows from Eqs. (154) and (155) that the FS wavenumbers

$$2k_\pm^2 = \beta_{1e}(\beta_{1e} + 2\gamma P_1) + \beta_{2e}(\beta_{2e} + 2\gamma P_2)$$

#4717 - $15.00 US Received 1 July 2004; revised 30 September 2004; accepted 1 October 2004

$$\pm\left\{[\beta_{1e}(\beta_{1e}+2\gamma P_1)-\beta_{2e}(\beta_{2e}+2\gamma P_2)]^2 + 4[4\beta_{1e}\beta_{2e}(\gamma\varepsilon)^2 P_1 P_2]\right\}^{1/2}. \quad (156)$$

By proceeding as described before Eq. (144), one can show that

$$G_1 = \frac{\cos(k_+z)}{1-\alpha_{1+}/\alpha_{1-}} + \frac{i\sigma\beta_{1e}\sin(k_+z)}{k_+(1-\alpha_{1+}/\alpha_{1-})} + \frac{\cos(k_-z)}{1-\alpha_{1-}/\alpha_{1+}} + \frac{i\sigma\beta_{1e}\sin(k_-z)}{k_-(1-\alpha_{1-}/\alpha_{1+})}, \quad (157)$$

$$H_1 = \frac{\sigma\cos(k_+z)}{1-\alpha_{1+}/\alpha_{1-}} + \frac{ik_+\sin(k_+z)}{\beta_{1e}(1-\alpha_{1+}/\alpha_{1-})} + \frac{\sigma\cos(k_-z)}{1-\alpha_{1-}/\alpha_{1+}} + \frac{ik_-\sin(k_-z)}{\beta_{1e}(1-\alpha_{1-}/\alpha_{1+})}, \quad (158)$$

$$G_2 = \frac{\alpha_{1+}\cos(k_+z)}{1-\alpha_{1+}/\alpha_{1-}} + \frac{i\sigma\alpha_{1+}\beta_{1e}\sin(k_+z)}{k_+(1-\alpha_{1+}/\alpha_{1-})} + \frac{\alpha_{1-}\cos(k_-z)}{1-\alpha_{1-}/\alpha_{1+}} + \frac{i\sigma\alpha_{1-}\beta_{1e}\sin(k_-z)}{k_-(1-\alpha_{1-}/\alpha_{1+})}, \quad (159)$$

$$H_2 = \frac{\sigma\alpha_{1+}\beta_{1e}\cos(k_+z)}{\beta_{2e}(1-\alpha_{1+}/\alpha_{1-})} + \frac{i\alpha_{1+}k_+\sin(k_+z)}{\beta_{2e}(1-\alpha_{1+}/\alpha_{1-})} + \frac{\sigma\alpha_{1-}\beta_{1e}\cos(k_-z)}{\beta_{2e}(1-\alpha_{1-}/\alpha_{1+})} + \frac{i\alpha_{1-}k_-\sin(k_-z)}{\beta_{2e}(1-\alpha_{1-}/\alpha_{1+})}, \quad (160)$$

where the auxiliary parameters

$$\alpha_{1\pm} = [k_\pm^2 - \beta_{1e}(\beta_{1e}+2\gamma P_1)]/2\beta_{1e}\gamma\varepsilon(P_1P_2)^{1/2}. \quad (161)$$

Because the subscripts $\pm$ in Eqs. (157)–(160) label the wavenumbers (156) and auxiliary parameters (161), rather than the sidebands, the $\pm$ terms have the same form. It follows from this observation, Eqs. (157)–(160), and the inversion formulas $C_{j+} = (G_j + H_j)/2$ and $C_{j-}^* = (G_j - H_j)/2$, that

$$C_{1-}^* = \frac{(1-\sigma)\cos(k_+z)}{2(1-\alpha_{1+}/\alpha_{1-})} + \left(\frac{\sigma\beta_{1e}}{k_+} - \frac{k_+}{\beta_{1e}}\right)\frac{i\sin(k_+z)}{2(1-\alpha_{1+}/\alpha_{1-})} + (+\leftrightarrow -), \quad (162)$$

$$C_{1+} = \frac{(1+\sigma)\cos(k_+z)}{2(1-\alpha_{1+}/\alpha_{1-})} + \left(\frac{\sigma\beta_{1e}}{k_+} + \frac{k_+}{\beta_{1e}}\right)\frac{i\sin(k_+z)}{2(1-\alpha_{1+}/\alpha_{1-})} + (+\leftrightarrow -), \quad (163)$$

$$C_{2-}^* = \frac{\alpha_{1+}(1-\sigma\beta_{1e}/\beta_{2e})\cos(k_+z)}{2(1-\alpha_{1+}/\alpha_{1-})} + \left(\frac{\sigma\beta_{1e}}{k_+} - \frac{k_+}{\beta_{2e}}\right)\frac{i\alpha_{1+}\sin(k_+z)}{2(1-\alpha_{1+}/\alpha_{1-})}, \quad (164)$$

$$C_{2+} = \frac{\alpha_{1+}(1+\sigma\beta_{1e}/\beta_{2e})\cos(k_+z)}{2(1-\alpha_{1+}/\alpha_{1-})} + \left(\frac{\sigma\beta_{1e}}{k_+} + \frac{k_+}{\beta_{2e}}\right)\frac{i\alpha_{1+}\sin(k_+z)}{2(1-\alpha_{1+}/\alpha_{1-})}. \quad (165)$$

For brevity $(+\leftrightarrow -)$ was omitted from Eqs. (164) and (165). Formulas (162)–(165) define the first and second columns of the transfer matrix. One can deduce formulas for the elements of the third and fourth columns by interchanging the subscripts 1 and 2.

Appendix B: Actions, Commutators and Reciprocity

In Sections 6 and 7 the input–output relation for the (quantum) mode operators was written in the form

$$B = MA, \quad (166)$$

#4717 - $15.00 US Received 1 July 2004; revised 30 September 2004; accepted 1 October 2004

where A is the vector of input operators, B is the vector of output operators and $M = [\mu_{jk}]$ is the transfer (Green) matrix. The commutator conservation equations $[b_j, b_k^\dagger] = [a_j, a_k^\dagger] = \delta_{jk}$ were used to show that

$$\sum_k |\mu_{jk}|^2 s_{jk} = 1, \tag{167}$$

where $s_{jk} = 1$ if operators j and k are of the same type, and $s_{jk} = -1$ if they are of different types. The two- and three-mode limits of Eq. (167) were stated in Eqs. (74), (89), (103) and (104). They are all consistent with the MRW equation (11), which was derived for the (classical) wave amplitudes and describes the conservation of wave action. This agreement might lead one to conclude that the commutator conservation equations and the MRW equation are different (quantum and classical) manifestations of the same physical law. However, such a conclusion is false. Equation (167) involves the rows of the Green matrix. Because the MRW equation is valid for arbitrary input conditions, it must also be valid when only one of the input waves has nonzero amplitude. By considering such input conditions, one finds that the matrix element (Green function) μ_{jk} describes the effect on mode j of a unit input to mode k and, hence, that the individual MRW equations

$$\sum_j |\mu_{jk}|^2 s_{jk} = 1, \tag{168}$$

which are the constituents of Eq. (11), follow from the columns of M. Hence, the MRW equation follows from the commutator conservation equations, which apply to any system, and the assumption of reciprocity ($\mu_{jk} = \mu_{kj}$), which depends on the symmetries of specific systems.

Consider a system governed by the linear equation

$$d_z B = LB, \tag{169}$$

where B is a vector of operators and L is a constant matrix. It is useful to expand the solution of Eq. (169) in terms of the eigenvectors E of the related equation $LE = \lambda E$. Let F be an eigenvector of the adjoint equation $L^\dagger F = \lambda^* F$. Then the solution of Eq. (169) can be written in the form

$$b_j(z) = \sum_n e_j^{(n)} f_k^{(n)*} \exp[\lambda^{(n)} z] b_k(0), \tag{170}$$

where b_j is a component of B and the superscript (n) labels the eigenvalues and associated eigenvectors. In Eq. (166) $a_k = b_k(0)$. It follows from solution (170) that

$$\mu_{jk} = \sum_n e_j^{(n)} f_k^{(n)*} \exp[\lambda^{(n)} z]. \tag{171}$$

For the special case in which L is hermitian (self-adjoint), the eigenvalues $\lambda^{(n)}$ are real, the adjoint eigenvectors $F^{(n)}$ are equal to the eigenvectors $E^{(n)}$, and $\mu_{jk} = \mu_{kj}^*$. Although amplitude reciprocity ($\mu_{jk} = \mu_{kj}$) does not exist for a complex system, the existence of modulus reciprocity ($|\mu_{jk}| = |\mu_{kj}|$) is sufficient to establish the MRW equation.

In the context of PA, it follows from Eqs. (7)–(10) that the coefficient matrix

$$L = \begin{bmatrix} -i\delta_1 & -i\alpha & -i\beta & -i\beta \\ i\alpha & i\delta_2 & i\beta & i\beta \\ -i\beta & -i\beta & -i\delta_3 & -i\gamma \\ i\beta & i\beta & i\gamma & i\delta_4 \end{bmatrix}, \tag{172}$$

where $\delta_1 = \beta_{1-} + \gamma P_1$, the definitions of the other diagonal elements are similar, and α, β and γ are abbreviations for γP_1, $\gamma\varepsilon(P_1 P_2)^{1/2}$ and γP_2, respectively. It is clear from Eq. (172) that L is not self-adjoint. However, the non-diagonal elements of L do exhibit the symmetry

$$l_{kj} = l_{jk} s_{jk}. \tag{173}$$

#4717 - $15.00 US Received 1 July 2004; revised 30 September 2004; accepted 1 October 2004

Inspections of the Green matrices for the two-mode and (some specific) four-mode processes [Eqs. (17), (23), (29), (34), (35) and (36)] show that the symmetry of the coefficient matrix is imparted to specific Green matrices. It is not difficult to show that the Green matrix always has this symmetry.

The solution of Eq. (169) can be written in the form of Eq. (166), where $A = B(0)$ and $M = \exp(Lz) = \sum_n (Lz)^n/n!$. Consider each term in this series individually. The first term (I) has the same symmetry as L because all non-diagonal elements are zero. Suppose that the nth term also has this symmetry and let $l_{ij}^{(n)}$ denote the ijth element of L^n. Then

$$\begin{aligned} l_{ki}^{(n+1)} &= \sum_j l_{kj} l_{ji}^{(n)} \\ &= \sum_j l_{jk} s_{jk} l_{ij}^{(n)} s_{ij} \\ &= \sum_j l_{ij}^{(n)} l_{jk} s_{ij} s_{jk}. \end{aligned} \tag{174}$$

For each j, the second pair of terms on the right side of Eq. (174) equals s_{ik}. The sum of the first pair equals $l_{ik}^{(n+1)}$ (because L commutes with L^n). Hence, Eq. (174) is equivalent to the equation

$$l_{ki}^{(n+1)} = l_{ik}^{(n+1)} s_{ik}, \tag{175}$$

which has the same symmetry as Eq. (173). It follows from Eq. (175) and the principle of induction that

$$\mu_{kj} = \mu_{jk} s_{jk}. \tag{176}$$

Modulus reciprocity always exists for PA and, hence, the MRW equation is always valid. The preceding discussion shows clearly that the MRW equation is a consequence of the commutator conservation equations and the symmetry of the four-mode process on which PA is based.

#4717 - $15.00 US Received 1 July 2004; revised 30 September 2004; accepted 1 October 2004